(2)

THE OHIO STATE UNIVERSITY

DTIC FILE COPY

TM Scattering by a Variable Sheet Impedance in a Multilayered Slab

Matthew E. Peters and Edward H. Newman

The Ohio State University
ElectroScience Laboratory
Department of Electrical Engineering
Columbus, Ohio 43212

Technical Report 721566-1
Contract N00014-89-J-1007
March 1990

Office of Naval Research
800 North Quincy Street
Arlington, VA 22217-5000

NOTICES

When Government drawings, specifications, or other data are used for any purpose other than in connection with a definitely related Government procurement operation, the United States Government thereby incurs no responsibility nor any obligation whatsoever, and the fact that the Government may have formulated, furnished, or in any way supplied the said drawings, specifications, or other data, is not to be regarded by implication or otherwise as in any manner licensing the holder or any other person or corporation, or conveying any rights or permission to manufacture, use, or sell any patented invention that may in any way be related thereto.

50272-101

REPORT DOCUMENTATION PAGE	1. REPORT NO.	2.	3. Recipient's Accession No.

4. Title and Subtitle
TM Scattering by a Variable Sheet Impedance in a Multilayered Slab

5. Report Date
March 1990

6.

7. Author(s)
Matthew E. Peters and Edward H. Newman

8. Performing Org. Rept. No.
721566-1

9. Performing Organization Name and Address
The Ohio State University
ElectroScience Laboratory
1320 Kinnear Road
Columbus, OH 43212

10. Project/Task/Work Unit No.

11. Contract(C) or Grant(G) No.
(C) N00014-89-J-0007
(G)

12. Sponsoring Organization Name and Address
Office of Naval Research
800 North Quincy Street
Arlington, VA 22217-5000

13. Report Type/Period Covered
Technical Report

14.

15. Supplementary Notes

16. Abstract (Limit: 200 words)

The problem considered is two-dimensional ~~(2D)~~ transverse magnetic (TM) scattering by a variable sheet impedance in a multilayered slab. An integral equation is formulated for the sheet impedance in the multilayered slab. This integral equation is solved for the surface currents flowing on the sheet impedance using a spectral domain moment method (MM)/Green's function solution. The MM solution is outlined and expressions for the matrix elements are obtained. A user oriented computer code was written to implement the solution. Numerical results are obtained and are compared with measured or previously calculated results.

17. Document Analysis a. Descriptors
DIELECTRICS, Computer [illegible]
SCATTERING, Mathematical [illegible]
MOMENT METHODS, moments
~~RCS~~
~~2-D~~

b. Identifiers/Open-Ended Terms

c. COSATI Field/Group

18. Availability Statement	19. Security Class (This Report)	21. No. of Pages
A. Approved for public release; Distribution is unlimited.	Unclassified	73
	20. Security Class (This Page) Unclassified	22. Price

(See ANSI-Z39.18) *See Instructions on Reverse* OPTIONAL FORM 272 (4-77)
Department of Commerce

TABLE OF CONTENTS

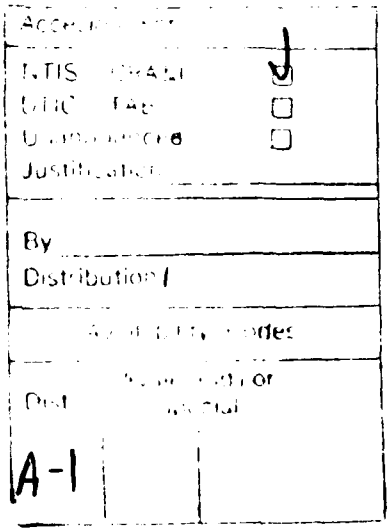

LIST OF FIGURES

CHAPTER I

INTRODUCTION

This report presents a moment method (MM) [1] [2] solution to two-dimensional (2D) transverse magnetic (TM) scattering by a variable sheet impedance in a multilayered slab. An integral equation is derived for the sheet impedance in the multilayered slab. This integral equation is solved for the surface currents flowing on the sheet impedance by employing a spectral domain MM/Green's function solution [3]. This solution is preferred because the Green's function accounts for the presence of the multilayered slab. Also, the fields in each layer of the multilayered slab can be easily expanded as plane wave spectra, thus the MM/Green's function solution is carried out in the spectral domain. A user oriented computer code was written to implement this solution and numerical results are presented.

A sheet impedance is a model for an electrically thin dielectric layer. The sheet impedances considered here can be variable, but they must be non-constant over a single finite range. The multilayered slab is planar and extends infinitely in all directions. The slab layers are of dielectric/ferrite materials which may be either lossy or lossless. The geometry of the sheet impedance and the multilayered slab is shown in Figure 1 in Chapter II. The problem is to compute the 2D scattering by this geometry from a TM incident plane wave.

The MM solution presented in this report is useful in that it allows for the analysis of scattering from isolated scattering points and variable sheet imped-

ances. For example, scattering from a single sheet impedance discontinuity can be computed, as well as scattering from a tapered sheet impedance where the taper occurs over a finite width. Also, scattering from a finite width sheet impedance variation can be computed. Finally, the sheet impedance may be located in a multilayered slab, on a half plane, or entirely in free space, and the scattering from these configurations can be computed.

The MM solution is begun by considering the sheet impedance and multilayered slab to be illuminated by a TM plane wave incident from the angle ϕ_0. The variable sheet impedance is replaced by the parallel combination of two sheet impedances. One sheet impedance will be constant while the other sheet impedance will be variable and/or constant and will produce the scattered field. Next, the equivalence theorem is used to replace the "scattering" sheet impedance by an unknown surface current $\mathbf{J}_s$. The condition that the total field is the sum of the incident field and the scattered field yields the integral equation for $\mathbf{J}_s$. The unknown surface current $\mathbf{J}_s$ is expanded in terms of N known basis functions of unknown strengths. The N coefficients in this expansion are then determined by the moment method. The scattered field is the sum of the individual fields of the N basis functions multiplied by their respective strengths.

Some previous work has been published on the impedance sheet approximation and resistive and impedance sheet scattering. Harrington and Mautz [1] presented the impedance sheet approximation and applied it in a MM solution for TM scattering by a thin dielectric shell. Senior [5] computed edge-on TM backscattering from a uniform resistive sheet half plane in free space. Senior [6] also analyzed backscattering from finite width resistive strips with attention focused on TM scattering near grazing incidence. Again, his analysis concerned strips with uniform resistance. Richmond [7] presented a MM solution for TM scattering by a finite

width electrically thin dielectric strip. His solution used basis functions incorporating known physical properties of the problem geometry into the MM solution. The MM solution presented in this report makes use of similar basis functions. Newman [8] [9] used a MM/Green's function solution to solve for scattering by a dielectric/ferrite cylinder in the presence of a perfectly conducting half plane. This solution can be used to model a PEC half plane with a variable impedance taper region at its edge. Newman and Blanchard [10] solved for TM scattering by an impedance sheet extension of a parabolic cylinder using a MM/Green's function solution.

Asymptotic work employing the uniform theory of diffraction (UTD) [11] has also been done in the analysis of thin dielectric/ferrite slabs. Rojas and Pathak [12] [13] analyzed diffraction by dielectric/ferrite half planes and strips. Rojas [14] also solved for scattering by an impedance discontinuity in a planar surface. Ly [15] presented a UTD solution for diffraction by junction edges formed between different electrically thin material slabs. For simple cases, the MM solution presented here was compared against the solution given in [15]. The agreement was always excellent.

The format of this report is as follows. The basic geometry of the problem is given in Chapter II. Chapter II also derives the integral equation and outlines the MM solution for the sheet impedance in the multilayered slab. Chapter III presents results of TM plane wave scattering by several different sheet impedances and multilayered slab geometries. When possible, these results were compared with measured or previously calculated results. Chapter IV briefly describes a computer code written to implement this MM solution and is intended as a user's manual for the code. Finally, Chapter V gives a summary of this report and presents ideas for further study.

CHAPTER II

THEORY

2.1 Introduction

This chapter develops the integral equation and moment method solution to the problem of 2D transverse magnetic (TM) plane wave scattering by a variable sheet impedance in a planar multilayered slab. The sheet impedance must be non-constant over a finite range for the MM solution presented here. The slab geometry is illustrated in Figure 1 and a sheet impedance model is shown in Figure 2.

The solution is obtained by first expressing the variable sheet impedance as the parallel combination of two sheet impedances. One sheet impedance will be constant while the other sheet impedance will be infinite, constant or variable over different ranges and produces the scattered field. The equivalence theorem is used to replace the scattering sheet impedance by an unknown surface current J_S. Next, the integral equation for J_S is obtained by enforcing the surface equivalence theorem on the sheet impedance surface. This integral equation is solved using a spectral domain moment method (MM)/Green's function solution which solves for the surface current J_s. Once J_s is known then the scattered fields are computed.

2.2 Problem Geometry and the Integral Equation

This section presents the development of an integral equation for the 2D transverse magnetic (TM) scattering by a variable sheet impedance, denoted $Z_S(x)$,

in a plane multilayered slab. As illustrated in Figure 1, the slab has K layers with permeability and permittivity (μ_k, ϵ_k) and thickness T_k; $k = 1, 2, ..., K$. The material parameters of the free space region above the multilayered slab are denoted (μ_0, ϵ_0) and the homogeneous region below the multilayered slab are denoted $(\mu_{K+1}, \epsilon_{K+1})$. All fields and currents are two dimensional (they are independent of y) and are time harmonic with the $e^{j\omega t}$ time variation suppressed. In addition, all electric fields and surface currents contain only a $\hat{y}$ - directed component so vector notation shall not be used and this polarization is implicit.

A sheet impedance is a model for an electrically thin dielectric slab. For example, Figure 2(a) shows a dielectric slab of thickness T and with material parameters (μ_0, ϵ). The wavenumber in the slab is $k = \omega\sqrt{\mu_0\epsilon}$. If $|k|T \ll 1$, then the slab is sufficiently thin that the electric field is essentially constant with respect to z. In this case, as illustrated in Figure 2(b), the thin dielectric slab can be replaced by the zero thickness sheet impedance [10]

$$Z_S = \frac{1}{j\omega(\epsilon - \epsilon_0)T}. \tag{2.1}$$

Although Figure 2(a) shows a homogeneous dielectric slab of uniform thickness, Equation (2.1) also applies to a slab in which T and/or ϵ are functions of x.

The sheet impedances considered here have the property that for some ranges of x, $Z_S(x) = Z_{S0}$ is constant, while for other ranges of x, $Z_S(x)$ is an arbitrary function of x. Furthermore, the range over which $Z_S(x)$ is non-constant (Z_{S0} or otherwise) must be finite to allow for a feasible sub-domain basis function expansion in this region. Some typical $Z_S(x)$ are shown in Figure 3. Figure 3(a) shows the most general sheet impedance with an arbitrary variation for $0 \leq x \leq L$ and

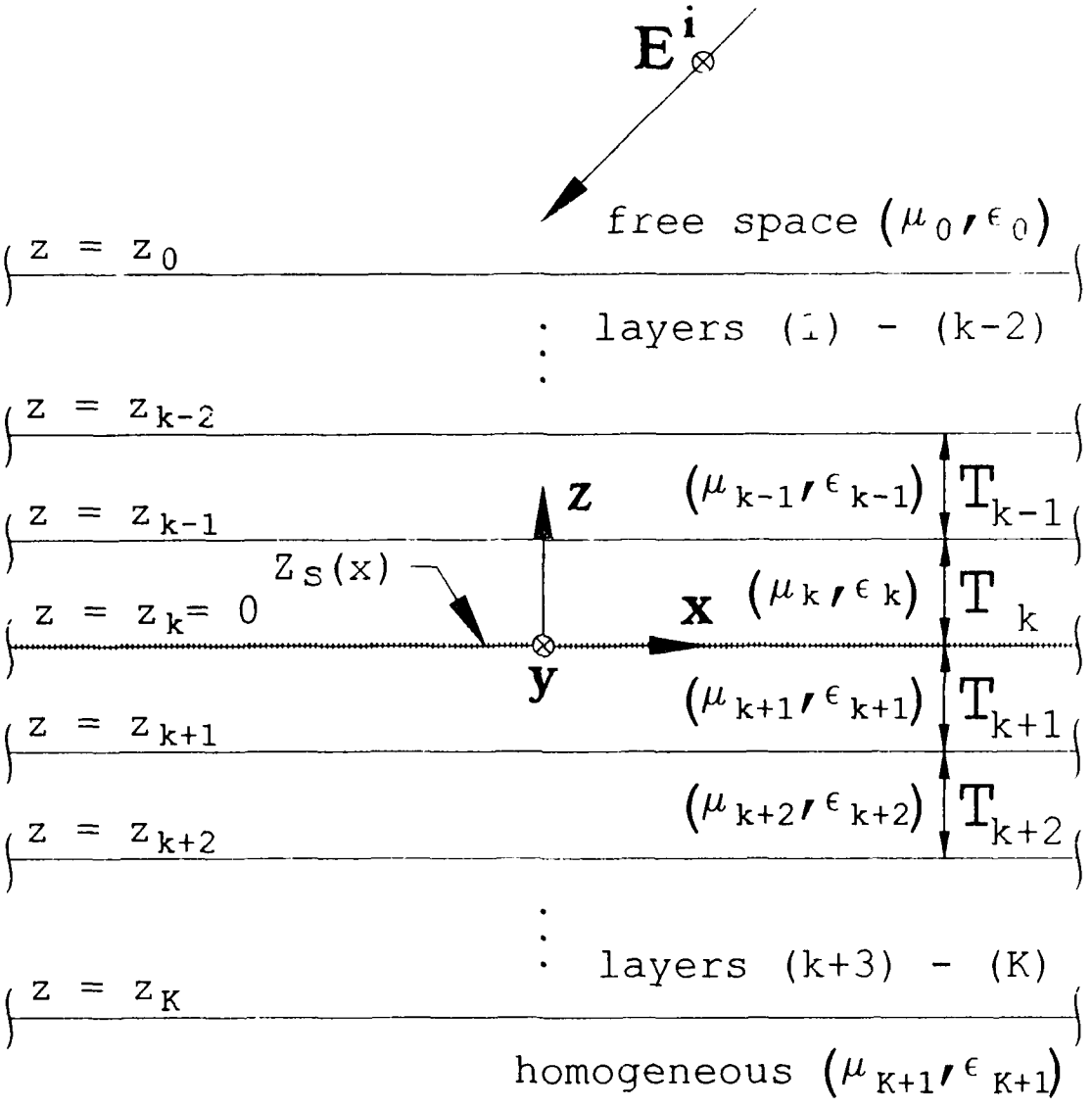

Figure 1: Multilayered slab and sheet impedance geometry.

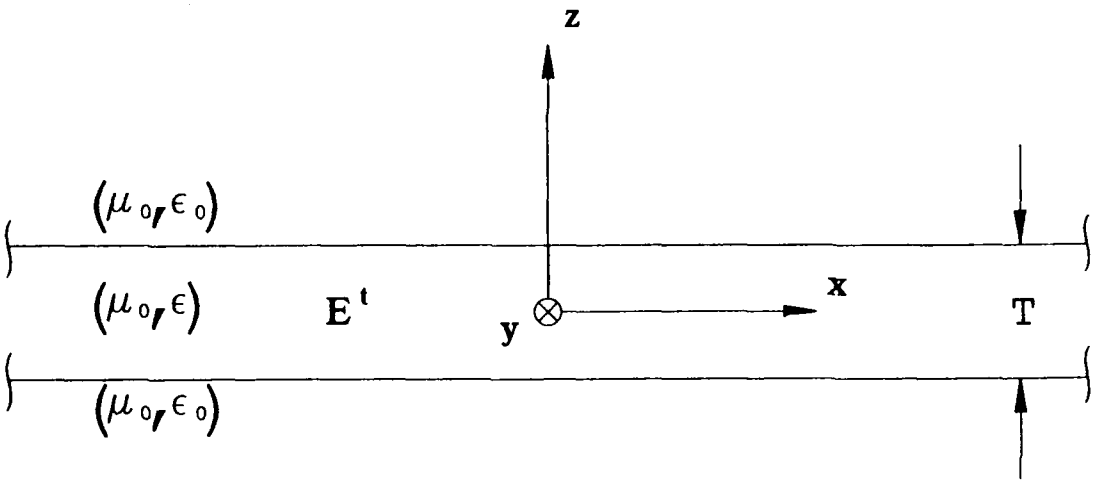

E^t = total electric field

(a)

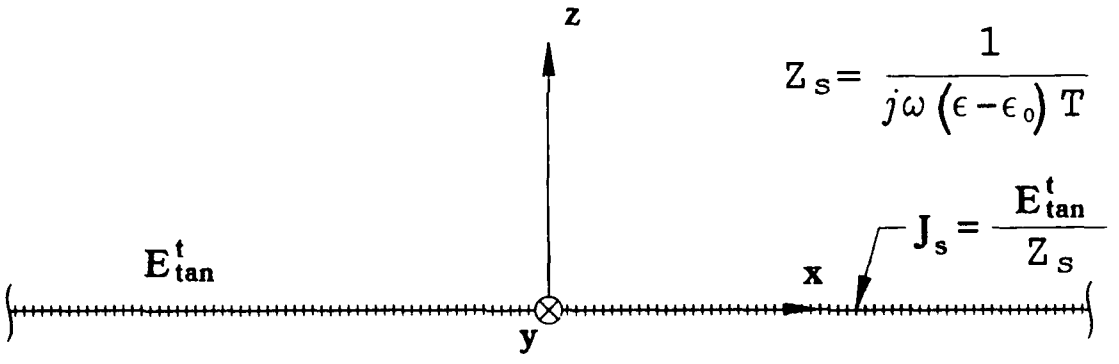

E^t_{tan} = total tangential electric field

(b)

Figure 2: Sheet impedance approximation through the equivalence theorem.

which is constant at Z_{S0} or Z_A outside this range. For example, in Figure 3(b)

$$Z_S(x) \quad \begin{cases} Z_{S0} & \text{if } x < 0 \\ Z_A & \text{if } 0 \leq x \leq L \\ Z_{S0} & \text{if } x > L. \end{cases} \tag{2.2}$$

The $Z_S(x)$ in Figures 3(c) and 3(d) differ from Z_{S0} over a semi-infinite range. However, $Z_S(x)$ is non-constant over a finite range of x, as required. In particular, for Figure 3(c)

$$Z_S(x) = \begin{cases} Z_{S0} & \text{if } x < 0 \\ Z_A & \text{if } x > 0, \end{cases} \tag{2.3}$$

and for Figure 3(d)

$$Z_S(x) \quad \begin{cases} Z_{S0} & \text{if } x < 0 \\ Z_T(x) & \text{if } 0 < x < L \\ Z_A & \text{if } x > L \end{cases} \tag{2.4}$$

where $Z_T(x)$ is an impedance taper function providing a smooth transition from Z_{S0} to Z_A over the range $0 < x < L$.

A simplified sketch of the multilayered slab containing $Z_S(x)$ is shown in Figure 4(a). Newman showed that the equivalent sheet impedance of a thin multilayered dielectric slab is given by the parallel combination of the sheet impedances of the individual layers [10]. Thus, the sheet impedance $Z_S(x)$ can be represented as the constant sheet impedance Z_{S0} in parallel with another sheet impedance, denoted $Z_{SP}(x)$. This equivalent geometry is shown in Figure 4(b). $Z_S(x)$ is given by

$$Z_S(x) = \frac{Z_{S0} Z_{SP}(x)}{Z_{S0} + Z_{SP}(x)} \tag{2.5}$$

from which it is found that $Z_{SP}(x)$ is given by

$$Z_{SP}(x) = \frac{Z_{S0} Z_S(x)}{Z_{S0} - Z_S(x)}. \tag{2.6}$$

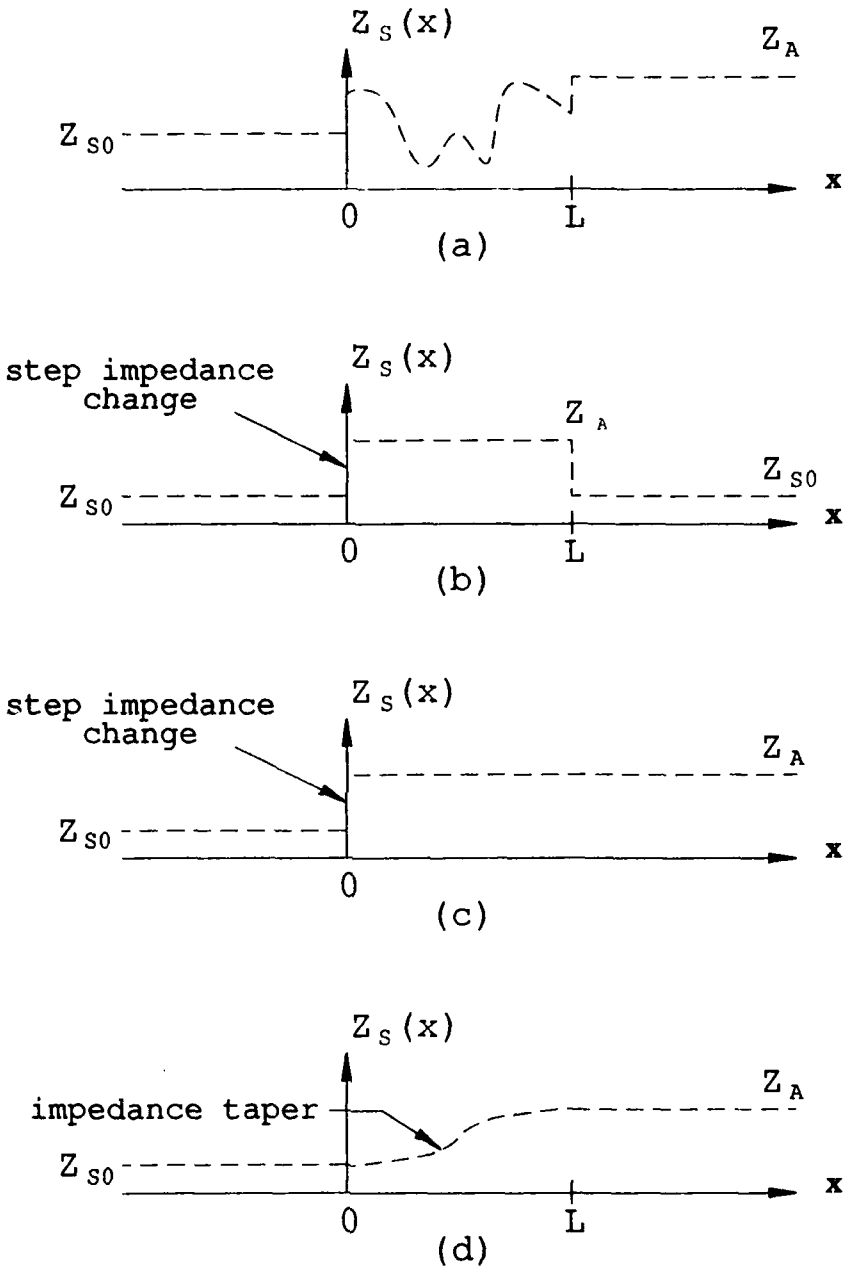

Figure 3: Typical sheet impedance variations.

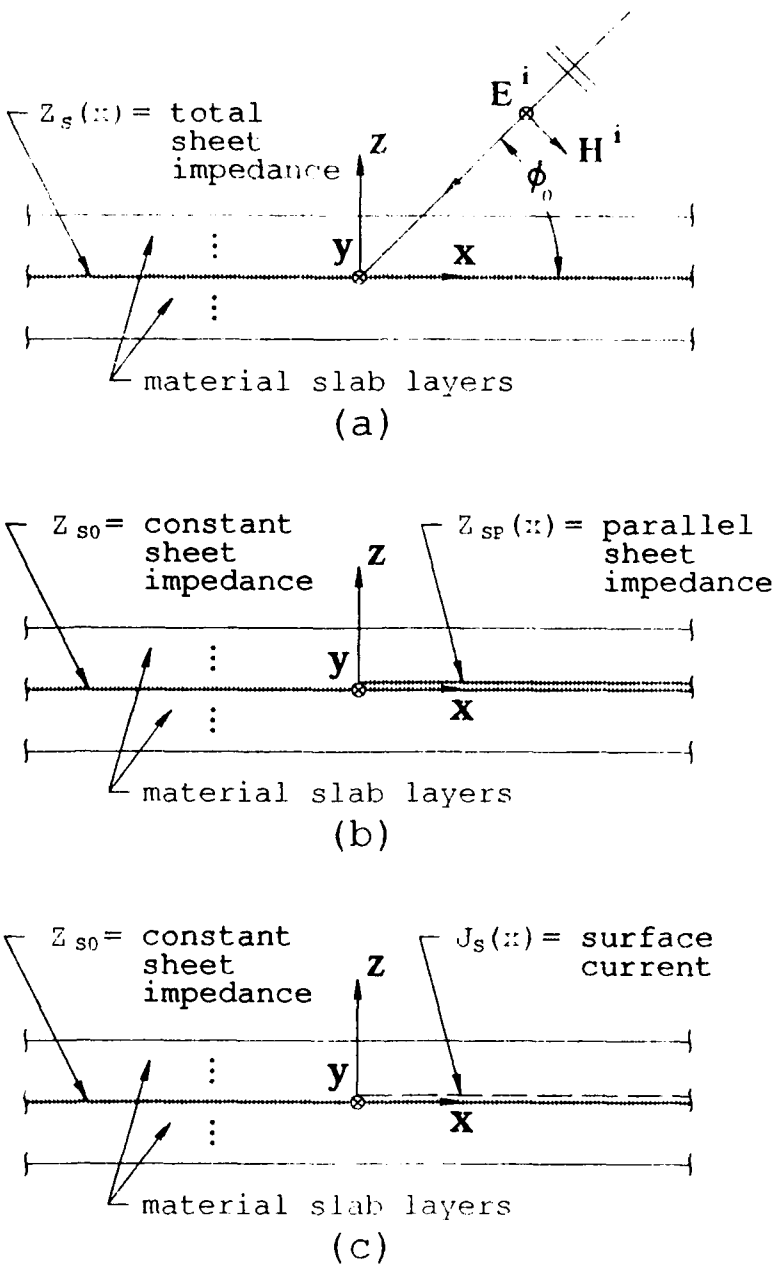

Figure 4: Equivalent geometries used in deriving the integral equation.

The scattered field is produced by the parallel sheet impedance $Z_{SP}(x)$, which is finite only where $Z_S(x) \neq Z_{S0}$. As illustrated in Figure 4(c) the volume equivalence theorem can be used to replace $Z_{SP}(x)$ by the surface current [10]

$$J_S(x) = \frac{E^t}{Z_{SP}(x)}, \tag{2.7}$$

where E^t is the total electric field on the surface of $Z_{SP}(x)$. Note that $J_S(x)$ is non-zero only where $Z_S(x) \neq Z_{S0}$, and that $J_S(x)$ radiates the scattered field E^s in the presence of the multilayered slab of Figure 4(c). The term "multilayered slab" refers to the K material layers and the sheet impedance Z_{S0}, but not $Z_{SP}(x)$. The total electric field is the sum of the incident plus the scattered field, i.e.,

$$E^t = E^i + E^s \tag{2.8}$$

where E^i is the field of the incident plane wave in the presence of the multilayered slab of Figure 4(c). *Combining Equations (2.7) and (2.8) yields*

$$-E^s + Z_{SP}(x)J_S(x) = E^i. \tag{2.9}$$

This is the basic integral equation for $J_S(x)$ because the electric field E^s can be expressed as

$$E^s = \int_l \bar{G}_y^s(x'|x,z)\, J_S(x')\, dx' \tag{2.10}$$

where $\bar{G}_y^s(x'|x,z)$ is the $\hat{y}$ component of the dyadic Green's function for the multilayered slab containing Z_{S0}. The $\hat{y}$ component of the dyadic Green's function is chosen because the surface current is $\hat{y}$ - directed. However, the dyadic Green's function will not be used in this analysis but is used only to show the form of the integral equation. Equation (2.9) will be solved for $J_S(x)$ in the next section using the MM.

2.3 Moment Method Solution

This section presents the development of the moment method solution to the integral equation developed in the previous section. The unknown surface current is approximated by a sum of N known basis functions of unknown strengths. The choice of the basis functions is discussed in Section 2.8. By taking an inner product of Equation (2.9) with a set of N weighting functions, a matrix equation is formed. The weighting functions will be chosen identical to the basis functions making this a Galerkin solution [1]. Finally, general expressions for the matrix elements are given. Note that all electric fields and surface currents are y - directed so vector notation is not used.

The moment method solution is begun by approximating the unknown surface current $J_S(x)$ as a sum of N known basis functions as follows:

$$J_S(x) = \sum_{n=1}^{N} I_n J_n \tag{2.11}$$

where the I_n are the N unknown strengths of each basis function and the J_n are the N known basis function expansion modes. Substituting the approximate surface current $J_S(x)$ of Equation (2.11) into Equation (2.9) it is obtained that

$$\sum_{n=1}^{N} I_n E_n + \sum_{n=1}^{N} I_n J_n Z_{SP}(x) = E^i \tag{2.12}$$

where E_n is the electric field of the n^{th} basis function J_n radiating in the presence of the multilayered slab (containing Z_{S0}). By taking the product of Equation (2.12) with each weighting function J_m for $m = 1, 2, ..., N$, and integrating then over the region of the weighting function, it is obtained that

$$\sum_{n=1}^{N} I_n \int_m E_n J_m \, dx + \sum_{n=1}^{N} I_n \int_m J_n J_m Z_{SP}(x) \, dx = \int_m E^i J_m \, dx. \tag{2.13}$$

The limit m on the integrals in the above equation denotes that the range of integration is over the region where thJ_m is non-zero. Equation (2.13) represents a set of N equations with N unknowns. This set of equations can be written compactly in matrix form as

$$[Z + \Delta Z]\,[I] = [V] \tag{2.14}$$

where $[Z + \Delta Z]$ is the $N \times N$ impedance matrix, $[I]$ is the length N vector of unknown strengths, and $[V]$ is the length N voltage excitation vector. The following equations define the elements of the impedance matrix and the voltage vector:

$$Z_{mn} = -\int_m E_n\, J_m\, dx \tag{2.15}$$

$$\Delta Z_{mn} = \int_m J_n\, J_m\, Z_{SP}(x)\, dx \tag{2.16}$$

$$V_m = \int_m E^i\, J_m\, dx. \tag{2.17}$$

Reciprocity can be applied to Equation (2.17) to obtain an expression for the voltage vector elements in terms of E_m, the electric field of the m^{th} weighting function J_m. The resulting reciprocal expression is

$$V_m = \int E_m\, J^i\, dv \tag{2.18}$$

where J^i is the impressed current that radiates the incident electric field E^i. The integral is over the volume of the impressed current.

The Z_{mn} impedance matrix contributions are distinctly different from the ΔZ_{mn} contributions. Equation (2.15) contains the electric field of the basis functions radiating in the presence of the multilayered slab. However, Equation (2.16) does not contain any electric fields. The Z_{mn} terms result from the field of the basis functions in Equation (2.9), whereas the ΔZ_{mn} terms result directly from the basis functions. As a result, the Z_{mn} terms require further evaluation, but the

ΔZ_{mn} terms can be evaluated directly from Equation (2.16) for known basis and weighting functions and surface impedance.

Note that both Equations (2.15) and (2.18) contain the electric fields of the basis functions and weighting functions radiating in the presence of the multilayered slab. The next section develops expressions for these electric fields and uses them to evaluate the impedance matrix elements.

2.4 Evaluation of the Impedance Matrix Elements

This section obtains an exact integral expression for the impedance matrix elements from the general expression given by Equation (2.15) in the preceeding section. An expression for the total electric field of the basis function J_n radiating in the presence of the multilayered slab will be developed using the plane wave expansion method [16]. This expression will be used in the evaluation of the matrix elements of Equations (2.15) and (2.18). This section evaluates Equation (2.15) in the spectral domain.

A separate plane wave expansion for the fields is used in each layer of the slab, in the free space region above the slab, and in the homogeneous region below the slab. Thus, for a K layered slab, there will exist $K + 2$ separate regions, each with its own plane wave expansion. In the following analysis, the notation for the subscript and superscript k is:

- $k = 0$ implies the free space region above the multilayered slab,
- $k = 1, 2, ..., K$ implies the k^{th} layer of the multilayered slab, and
- $k = K + 1$ implies the homogeneous region below the multilayered slab.

The basis functions J_n are assumed to be Fourier transformable with the Fourier transform pair defined as

$$\tilde{J}_n^{\pm} = \int_{-\infty}^{+\infty} J_n \, e^{\pm j\beta x} \, dx \tag{2.19}$$

$$J_n = \frac{1}{2\pi} \int_{-\infty}^{+\infty} \tilde{J}_n^{\pm} \, e^{\mp j\beta x} \, d\beta. \tag{2.20}$$

$\tilde{J}_n^{\pm}$ are referred to as the "plus" and "minus" Fourier transforms of J_n.

The surface current lies on the interface between two regions so each region can be considered source free. Thus, the electric and magnetic fields in each region must satisfy the source free vector wave equation

$$(\nabla^2 + k_k^2) \left\{ \begin{array}{c} \mathbf{E_n^k} \\ \mathbf{H_n^k} \end{array} \right\} = 0 \tag{2.21}$$

where $k_k = \omega\sqrt{\mu_k \epsilon_k}$ is the wave number of the k^{th} region. The total $\hat{y}$ - polarized electric field in region k, produced by J_n radiating in the presence of the multilayered slab, is expressed as a continuous spectrum of plane waves, i.e.,

$$E_n^k(x,z) = \int_{-\infty}^{+\infty} \left[A_n^k(\beta) \, e^{-\gamma_k z} + B_n^k(\beta) \, e^{\gamma_k z} \right] e^{j\beta x} \, d\beta \tag{2.22}$$

where $A_n^k(\beta)$ and $B_n^k(\beta)$ are spectral weighting functions to be determined, and γ_k is a propagation constant for waves travelling in the z direction. Applying Equation (2.21) to Equation (2.22) yields the separation equation

$$\gamma_k = \sqrt{\beta^2 - k_k^2} \quad ; \, \mathrm{Re}(\gamma_k) \geq 0 \, , \mathrm{Im}(\gamma_k) \geq 0. \tag{2.23}$$

This relates the propagation constant γ_k to the plane wave spectrum parameter β. The conditions on γ_k insure that the wave decays in the direction it travels. In this manner, the term of Equation (2.22) associated with $A_n^k(\beta)$ is an upward

travelling wave and the term associated with $B_n^k(\beta)$ is a downward travelling wave. Expressions for the magnetic field are obtained from Maxwell's equation

$$\nabla \times \mathbf{E} = j\omega\mu\mathbf{H}. \tag{2.24}$$

Applying Equation (2.24) to Equation (2.22) the following magnetic field is obtained:

$$H_{nx}^k(x,z) = \frac{1}{j\omega\mu_k}\int_{-\infty}^{+\infty}\gamma_k\left[A_n^k(\beta)\,e^{-\gamma_k z} - B_n^k(\beta)\,e^{\gamma_k z}\right]e^{j\beta x}\,d\beta \tag{2.25}$$

$$H_{nz}^k(x,z) = \frac{1}{\omega\mu_k}\int_{-\infty}^{+\infty}\beta\left[A_n^k(\beta)\,e^{-\gamma_k z} + B_n^k(\beta)\,e^{\gamma_k z}\right]e^{j\beta x}\,d\beta. \tag{2.26}$$

Next, the functions $A_n^k(\beta)$ and $B_n^k(\beta)$ must be determined. These functions are determined by enforcing the following conditions on the fields:

1. the radiation condition as $z \to \infty$,

2. continuity of the tangential electric field across each interface,

3. continuity of the tangential magnetic field across each interface except the $z = 0$ interface, and

4. discontinuity of the tangential magnetic field, by the total surface current produced by J_n, across the $z = 0$ interface, i.e.,

$$\hat{\mathbf{z}} \times \left[\mathbf{H}_n^k - \mathbf{H}_n^{k+1}\right] = \mathbf{J}_n^t \tag{2.27}$$

where k and $k+1$ represent the regions immediately above and below the $z = 0$ interface respectively, and $\mathbf{J}_n^t$ is the total surface current produced by J_n.

$\mathbf{J}_n^t$ contains only a $\hat{y}$ - directed component which at the $z = 0$ interface can be written as

$$J_n^t = \frac{E_n^k(x,0)}{Z_S(x)} = J_n + \frac{E_n^k(x,0)}{Z_{S0}}. \tag{2.28}$$

In Equation (2.28) E_n^{k+1} could have been used instead of E_n^k since the tangential electric field is continuous across the $z = 0$ interface.

Enforcing the above conditions on the fields of Equations (2.22) and (2.25), and substituting Equations (2.20) and (2.22) into Equation (2.28), the electric field E_n^k is obtained in terms of $\tilde{J}_n$. In Appendix A it is shown that the electric field at the $z = 0$ interface is given by

$$E_n^k(x,0) = -\frac{1}{2\pi}\int_{-\infty}^{+\infty} F(\beta)\,\tilde{J}_n^-\,e^{j\beta x}\,d\beta \tag{2.29}$$

where $F(\beta)$ is a spectral function specific to the multilayered slab geometry. $F(\beta)$ can be viewed as a spectral domain Green's function. See Appendix A for the determination of $F(\beta)$ for several simple geometries, such as the sheet impedance located in a $K = 2$ layered slab, on a material half space, and entirely in free space.

The impedance matrix elements are obtained by substituting Equation (2.29) into Equation (2.15) to obtain

$$Z_{mn} = \frac{1}{2\pi}\int_m\int_{-\infty}^{+\infty} F(\beta)\,\tilde{J}_n^-\,e^{j\beta x}\,J_m\,d\beta\,dx. \tag{2.30}$$

Reversing the order of integrations, and employing the Fourier transform relationship of Equation (2.19), it is finally obtained that

$$Z_{mn} = \frac{1}{2\pi}\int_{-\infty}^{+\infty} F(\beta)\,\tilde{J}_m^+\,\tilde{J}_n^-\,d\beta. \tag{2.31}$$

This is the so-called spectral integral formula for the impedance matrix elements. This integral expression is preferable to using Equation (2.10) in Equation (2.15) because there is only one integration. Furthermore, the dyadic Green's function

for the multilayered slab need not be determined. However, the function $F(\beta)$ must be determined. Note that determining the impedance matrix elements for different multilayered slab geometries is trivial. All that needs to be done is to insert the $F(\beta)$ corresponding to the geometry of interest into Equation (2.31). Thus, different spectral functions $F(\beta)$ can be used for different geometries.

2.5 Numerical Evaluation of the Impedance Matrix

The impedance matrix elements given by Equation (2.31) will be evaluated numerically. There are two problems encountered in the numerical evaluation of the impedance matrix. The first problem is the CPU time required for the computation of the impedance matrix. The second problem is that surface wave poles produce singularities in the integrand of the spectral integral formula. This section discusses these problems.

2.5.1 CPU Time Reduction

The spectral integral formula for the impedance matrix elements is given by Equation (2.31). Noting the form of the equation, the re-evaluation of the same quantities can be eliminated by computing all the elements in a parallel fashion. Thus, the entire impedance matrix should be computed in just one numerical integration with a matrix multiplication performed inside the integral, i.e.,

$$\begin{bmatrix} Z_{11} & Z_{12} & \cdots & Z_{1N} \\ Z_{21} & Z_{22} & \cdots & Z_{2N} \\ \vdots & \vdots & \ddots & \vdots \\ Z_{N1} & Z_{N2} & \cdots & Z_{NN} \end{bmatrix} = \frac{1}{2\pi} \int_{-\infty}^{+\infty} F(\beta) \begin{bmatrix} \tilde{J}_1^1 \\ \tilde{J}_2^1 \\ \vdots \\ \tilde{J}_N^1 \end{bmatrix} \begin{bmatrix} \tilde{J}_1 & \tilde{J}_2 & \cdots & \tilde{J}_N \end{bmatrix} d\beta. \tag{2.32}$$

Note that in this evaluation of the impedance matrix, the quantities $F(\beta)$, $\tilde{J}_m^1$ and $\tilde{J}_n$ are evaluated only once at each value of β employed in the numerical

integration. This results in an immense savings in CPU time required for the impedance matrix computation.

2.5.2 Surface Wave Poles

The spectral function $F(\beta)$ in the expression for Z_{mn} of Equation (2.31) may contain poles which make the integrand singular. Physically, these poles correspond to surface waves that exist on the multilayered slab containing the constant sheet impedance Z_{S0}. The number of surface wave poles can increase with increasing frequency. Typically, for lossless layers, these poles lie on the Re(β) axis between k_0 and $k_{D_{max}}$ = the maximum wavenumber of a layer medium. For lossy layers, these poles will move into the second and fourth quadrants, but for only slightly lossy layers they will be close to the Re(β) axis. If the poles are close to or on the Re(β) axis, they will distort the numerical β integration for Z_{mn} unless the integration path is staggered around them as shown in Figure 5. This staggered contour will produce an accurate result since the staggered contour does not cross any poles, nor does it pass too closely to their singularities. This staggered contour method has worked well for Δ given by

$$\Delta = \begin{cases} 0.2 & \text{if } W < 5\lambda_{D_{min}} \\ \lambda_{D_{min}}/W & \text{otherwise} \end{cases} \tag{2.33}$$

where W is the width of the pulse basis function region and $\lambda_{D_{min}}$ is the wavelength in medium $k_{D_{max}}$. The contour then returns to the Re(β) axis around $1.2k_{D_{max}}$.

2.6 Evaluation of the Voltage Vector Elements

This section obtains an expression for the voltage vector elements from the expression given in Equation (2.17) for the case of a uniform incident plane wave. The geometry of the incident wave is shown in Figure 4(a). An impressed current

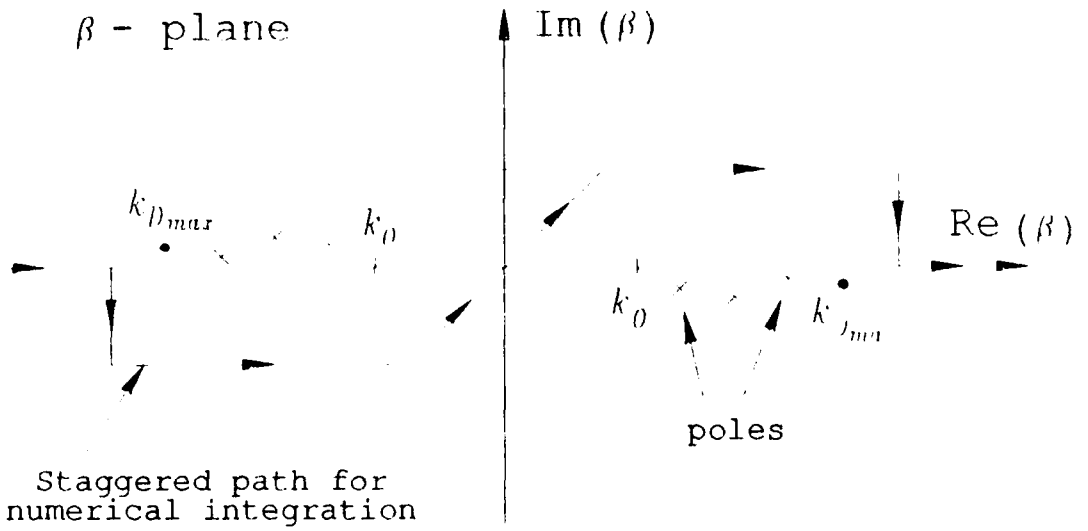

Figure 5: Integration contour for Z_{mn} in β plane.

source that radiates a plane wave in the far zone in free space will be defined so that the reciprocal expression of Equation (2.18) can be used. Finally, an expression for the far zone field of a basis function radiating in the presence of the multilayered slab will be obtained. This far zone field expression will be used in the evaluation of Equation (2.18) and also in the computation of the far zone scattered field. The formulation outlined here assumes that the wave is incident from the upper half space $z > 0$. A similar approach can be used if the wave is incident from the lower half space.

The incident plane wave illuminating the multilayered slab is

$$E^i = e^{jk_0(x\cos\phi_0 + z\sin\phi_0)}. \tag{2.34}$$

This field will be produced by the impressed current line source

$$J^i = \frac{\sqrt{8\pi k_0}}{\omega\mu_0} e^{-j\frac{\pi}{4}} \sqrt{\rho}\, e^{jk_0\rho} \tag{2.35}$$

located at the point (ρ, ϕ_0) in the limit as $\rho \to \infty$. It should be noted that the strength of J^i depends upon the distance ρ, so that E^i has unit amplitude near the origin.

Substituting Equation (2.35) into Equation (2.18) it is obtained that

$$V_m = -E_m \frac{\sqrt{8\pi k_0}}{\omega\mu_0} e^{-j\frac{\pi}{4}} \sqrt{\rho}\, e^{jk_0\rho} \tag{2.36}$$

where E_m is the field of J_m evaluated at (ρ, ϕ_0), the location of the impressed current source J^i. The method of stationary phase is used to asymptotically evaluate E_m [17] [18] in Appendix B. E_m is found to be of the form

$$E_m = P_m(\phi_0) \frac{e^{-jk_0\rho}}{\sqrt{\rho}} \tag{2.37}$$

where $P_m(\phi_0)$ is a function of ϕ_0 dependant upon the multilayered slab geometry. See Appendix B for the evaluation of E_m for several simple geometries. Substituting Equation (2.37) into Equation (2.36) the voltage vector elements are found to be

$$V_m = -P_m(\phi_0) \frac{\sqrt{8\pi k_0}}{\omega\mu_0} e^{-j\frac{\pi}{4}}. \tag{2.38}$$

This completes the discussion of the calculation of the voltage vector elements.

2.7 Computation of the Scattered Field

Once the impedance matrix and voltage vector are known, the current vector can be obtained using standard matrix algebra. Then, once the current vector is known, the far zone scattered field can be obtained as the sum of the far zone field of each basis function J_n multiplied by its respective strength I_n. Thus, the far zone scattered field is be given by

$$E^s = \sum_{n=1}^{N} I_n E_n^0 \tag{2.39}$$

where I_n is the strength of J_n and E_n^0 is the far zone field of J_n radiating in the presence of the multilayered slab. The far zone field of a basis function is determined asymptotically in Appendix B and is given by Equation (B.5). Substituting Equation (B.5) into Equation (2.39), the scattered field is found to be

$$E^s \quad \sum_{n=1}^{N} I_n P_n(\phi) \frac{e^{-jk_0\rho}}{\sqrt{\rho}} \tag{2.40}$$

where $P_n(\phi)$ is dependant on the multilayered slab geometry and is also determined in Appendix B and is given by Equation (B.6).

2.8 Basis and Weighting Functions

This section discusses the basis and weighting functions used in the MM solution. The weighting functions are chosen identical to the basis functions making this a Galerkin solution. It will be explained how the choice of basis functions is determined by the nature of the sheet impedance $Z_S(x)$. All basis functions are Fourier transformable, as required by the spectral integral formula for the impedance matrix elements. The basis functions and their Fourier transforms are presented below.

Recall that the surface current $J_S(x)$ is non-zero in the range of x where $Z_S(x) \neq Z_{S0}$. Therefore, $J_S(x)$ must be expanded in terms of basis functions in this range. Furthermore, the range where $Z_S(x) \neq Z_{S0}$ can be either finite or semi-infinite. However, the range where $Z_S(x)$ is non-constant must be finite to allow for a feasible subsectional basis function expansion in this range.

Figure 3(b) shows a case where $Z_S(x) \neq Z_{S0}$ over a finite range of x. In this case, $J_S(x)$ is expanded in subsectional basis functions over this range. Pulse functions are chosen as the subsectional basis functions in this MM solution. Figures 3(c) and 3(d) show cases where $Z_S(x) \neq Z_{S0}$ over a semi-infinite range of x. In

these cases it would be impossible to express $J_S(x)$ as an expansion of subsectional basis functions over the entire semi-infinite range because $N \rightarrow \infty$. To circumvent this problem, $J_S(x)$ is expanded in terms of pulse basis functions only in and near the range where $Z_S(x)$ is non-constant or discontinuous. In addition, $J_S(x)$ is expanded in terms of physical semi-infinite domain basis functions outside of this range. A physical basis function is a basis function with a variation dependant on a physical characteristic of the problem geometry. These basis functions incorporate known variations into the MM solution. Thus, some insight into the problem is required to choose this type of basis function. For example, a physical optics (PO) basis function is chosen to account for the current variation induced by the incident plane wave. Also, surface wave basis functions are chosen when surface waves can be supported by the sheet impedance. These are the two types of physical basis functions used in this MM solution. They are semi-infinite domain basis functions because they extend to infinity in the $+\hat{x}$ - direction. It is assumed that the current far enough away from any non-constant variations or discontinuities of $Z_S(x)$ can be approximated accurately by only the PO and surface wave basis functions because $Z_S(x)$ is constant in this range.

Figure 6 shows the choice and placement of basis functions needed for a proper and complete expansion of $J_S(x)$ for three typical variations of $Z_S(x)$. It should be noted that in Figures 6(b) and 6(c) surface wave basis functions should be included only if the multilayered slab geometry can support surface waves. However, surface wave basis functions need not be included (even if the geometry can support them) if the surface wave decays to insignificant strength in the pulse basis function region. If the slab layer is lossy enough, or the surface wave propagation constant provides rapid enough attenuation, then this will be the case. In these cases, the current variation near the non-constant or discontinuous sheet impedance, caused

by the attenuated surface wave, will be approximated well enough by the pulse basis functions alone.

If the range where $Z_S(x) \neq Z_{S0}$ is finite, then pulse basis functions are used over the entire range. If $Z_S(x) \neq Z_{S0}$ over a semi infinite range, then pulse basis functions are used in and near the range where $Z_S(x)$ is non-constant or discontinuous, i.e., they are used over a range starting where $Z_S(x)$ first deviates from Z_{S0}, and ending far enough beyond where $Z_S(x)$ has become constant once again that $J_S(x)$ can be approximated by only the PO and surface wave basis functions. In either case, the range where $J_S(x)$ is expanded in terms of pulse basis functions is finite. This finite range is divided into N segments and a pulse basis function is placed on each segment. The pulse basis functions are of the form

$$J_n = \begin{cases} 1 & \text{over segment } n \\ 0 & \text{otherwise.} \end{cases} \tag{2.41}$$

Applying the Fourier transform of Equation (2.19) to the pulse basis functions, the transforms are found to be

$$\tilde{J}_n^{\dagger} = \frac{2}{\beta} e^{+j\beta x_n} \sin(\beta \frac{w_n}{2}) \tag{2.42}$$

where x_n is the center of the n^{th} segment and w_n is the width of the n^{th} segment.

The PO basis function is used when $Z_S(x) \neq Z_{S0}$ over a semi-infinite range. It is used to model the current variation induced by a plane wave incident on a constant sheet impedance. The x variation of the incident plane wave is $e^{jk_0 x \cos\phi_0}$ where ϕ_0 is the angle of incidence. Thus, the PO basis function is chosen to be

$$J_n = \begin{cases} e^{jk_0 x \cos\phi_0} & \text{if } x > x_{PO} \\ 0 & \text{otherwise} \end{cases} \tag{2.43}$$

where x_{PO} is typically 0 or the value of x where the pulse basis functions stop. If the free space region $k = 0$ is viewed as a slightly lossy media in the limit as the

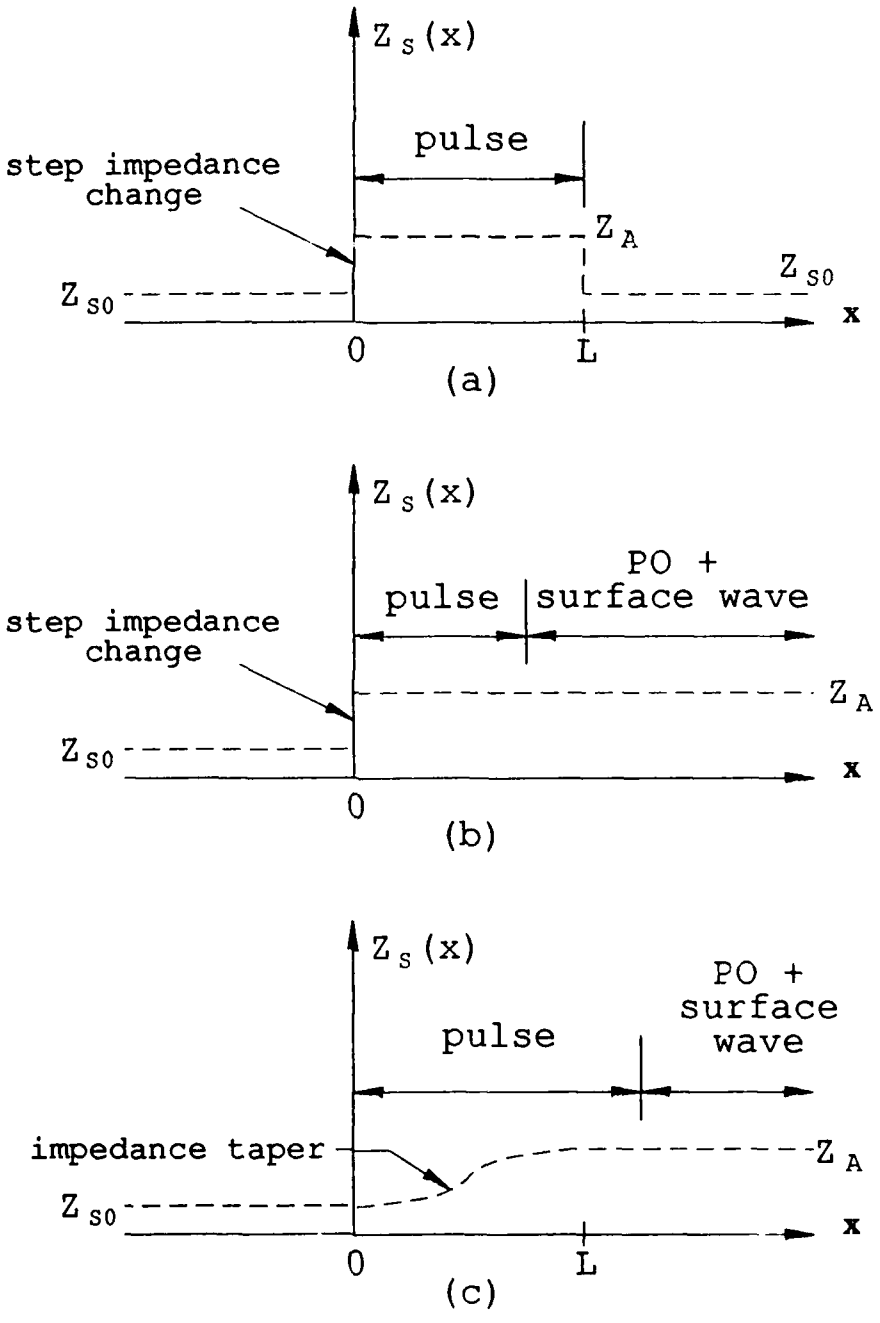

Figure 6: Choice of basis functions for typical $Z_S(x)$ variations.

loss vanishes, then J_n will be Fourier transformable with the transform

$$\tilde{J}_n^+ = \frac{e^{j(+\beta+k_0\cos\phi_0)x_{PO}}}{j(+\beta+k_0\cos\phi_0)}. \tag{2.44}$$

Note that the PO basis function depends on the incident angle ϕ_0. Therefore, each time the incident angle changes, as in a backscatter pattern computation, the impedance matrix changes. More specifically, as ϕ_0 changes, the rows and columns of the impedance matrix associated with the PO basis function must be recomputed.

The surface wave basis function is also used when $Z_S(x) \neq Z_{S0}$ over a semi-infinite range. However, it is used only when a surface wave can be supported by the multilayered slab geometry. Recall that if a surface wave exists and it decays quickly enough, then a surface wave basis function does not need to be included for that surface wave. The surface wave basis function is used to model the current variation associated with a surface wave, "launched" from the deviation of $Z_S(x)$ from Z_{S0}, which travels in the $+\hat{x}$ - direction. In general, more than one surface wave can exist. If a surface wave is launched, it will have the following x variation:

$$e^{-j\gamma_S x} \quad \text{where} \quad \begin{cases} \mathrm{Re}(\gamma_S) > 0 \\ \mathrm{Im}(\gamma_S) < 0 \end{cases} \tag{2.45}$$

where $j\gamma_S$ is the surface wave propagation constant. The conditions on γ_S insure that the surface wave decays as it travels in the $+\hat{x}$ - direction. The surface wave basis function is chosen to be

$$J_n \quad \begin{cases} e^{-j\gamma_S x} & \text{if } x > x_S \\ 0 & \text{otherwise} \end{cases} \tag{2.46}$$

where x_S is typically 0 or the value of x where the pulse basis functions stop. J_n is Fourier transformable with the transform

$$\tilde{J}_n^+ \quad \frac{e^{j(+\beta-\gamma_S)x_S}}{j(+\beta-\gamma_S)}. \tag{2.47}$$

To use surface wave basis functions, the surface wave propagation constants must first be obtained. However, it should be noted that surface waves will not always exist. If they do exist, the surface wave propagation constants for a multilayered slab geometry are the poles of the function $F(\beta)$ where Z_{S0} is replaced by the sheet impedance the surface waves exist on. $F(\beta)$ is given in Appendix A for several multilayered slab geometries. In general, solving for the surface wave poles will result in a transcendental equation which can be solved numerically. The surface wave poles must satisfy the conditions stated in Equation (2.45). When choosing surface wave basis functions, those associated with propagating and slowly decaying surface waves should be chosen first since they are the dominant modes.

In this MM solution, surface wave basis functions are included only in the case where $Z_S(x)$ is entirely in free space, i.e., no material layers exist. However, surface waves cannot exist on a purely real sheet impedance in free space [19]. In Figures 6(b) and 6(c), *if* $Im(Z_A) \neq 0$, *then a surface wave will travel in the* $+\hat{x}$ - direction along Z_A. In this case, solving for the poles of Equation (A.20) where $Z_{S0} \rightarrow Z_A$, the surface wave propagation constant is found to be

$$j\gamma_S = \pm jk_0\sqrt{1 - \frac{Z_0^2}{4Z_A^2}} \tag{2.48}$$

where $Z_0 = \sqrt{\frac{\mu_0}{\epsilon_0}}$ is the characteristic impedance of free space. The root of Equation (2.48) is chosen so that the conditions of Equation (2.45) are satisfied.

CHAPTER III

NUMERICAL RESULTS

This chapter presents results obtained from the MM procedure outlined in Chapter II. The results include computed backscatter from various sheet impedances and multilayered geometries. The results are compared with measurements and previously calculated results.

3.1 Convergence and Current Distribution Results

This section shows convergence data on the echo width scattered by a perfectly conducting half plane for edge-on incidence. Figure 7 shows the edge-on echo width versus the width of the pulse basis function region, labeled W in the figure. The PO basis function is required. The frequency is 300 MHz so that λ = 1 meter. Each pulse basis function is 0.1λ wide and the W is varied from 0 to 3λ. Thus, the number of pulses varies from 0 to 30 pulses. It can be seen that the echo width converges to within 0.25 dB of the exact value at a pulse region width of about 1λ. This appears to be the best this MM solution can do for a pulse basis function width of 0.1λ. If greater accuracy is desired, a smaller pulse width can be used.

Figure 8 shows the edge-on echo width versus the width of the individual pulse basis functions, labeled D in the figure. Once again, the PO basis function is used and the frequency is 300 MHz. The pulses are placed over the first wavelength (W = λ) and D is varied from 0.033 to 0.25. At D=0.033 there are 30 pulses and at

D=0.25 there are 4 pulses. The MM solution converges nicely, thus demonstrating the accuracy of the solution.

The MM current distribution for a typical basis function expansion is compared to the exact current distribution on the PEC half plane [5] in Figure 9. The MM current distribution uses a PO basis function starting at $x_{PO} = 0$. Also, 10 pulse basis functions of width 0.1λ each are used over the first wavelength of the PEC half plane. The frequency is 300 MHz ($\lambda = 1$ meter) and the current distribution is plotted over the first two wavelengths of the half plane. The MM and exact currents are in reasonable agreement with one another. For the range $0 \leq x \leq \lambda$, the current consists of pulses superimposed on the PO current, thus giving the distribution the slightly modified staircase shape. For $x > \lambda$ the current distribution consists only of the PO current. This can be seen in the constant magnitude and linear phase of the current in this region. It is interesting to note that the MM current at the center of the first pulse is about 1.44 times the exact current at this location. The exact current has a $\frac{1}{\sqrt{x}}$ dependance near the edge of the half plane. The average value of the exact current over the first pulse width divided by its value at the center of the first pulse is $\sqrt{2} \approx 1.41$. Thus, despite the appearance of the current plot, the MM current distribution does a very good job of approximating the exact current over the first pulse region.

3.2 Backscatter Versus Frequency Results

This section presents a comparison of measured backscatter from a sheet impedance located in a $K = 2$ layered slab with results obtained from this MM solution. Measured and computed echo width versus frequency are compared. The MM computations were obtained using an impedance matrix interpolation method [20]. The inserts in Figures 10 and 11 show the multilayered slab geome-

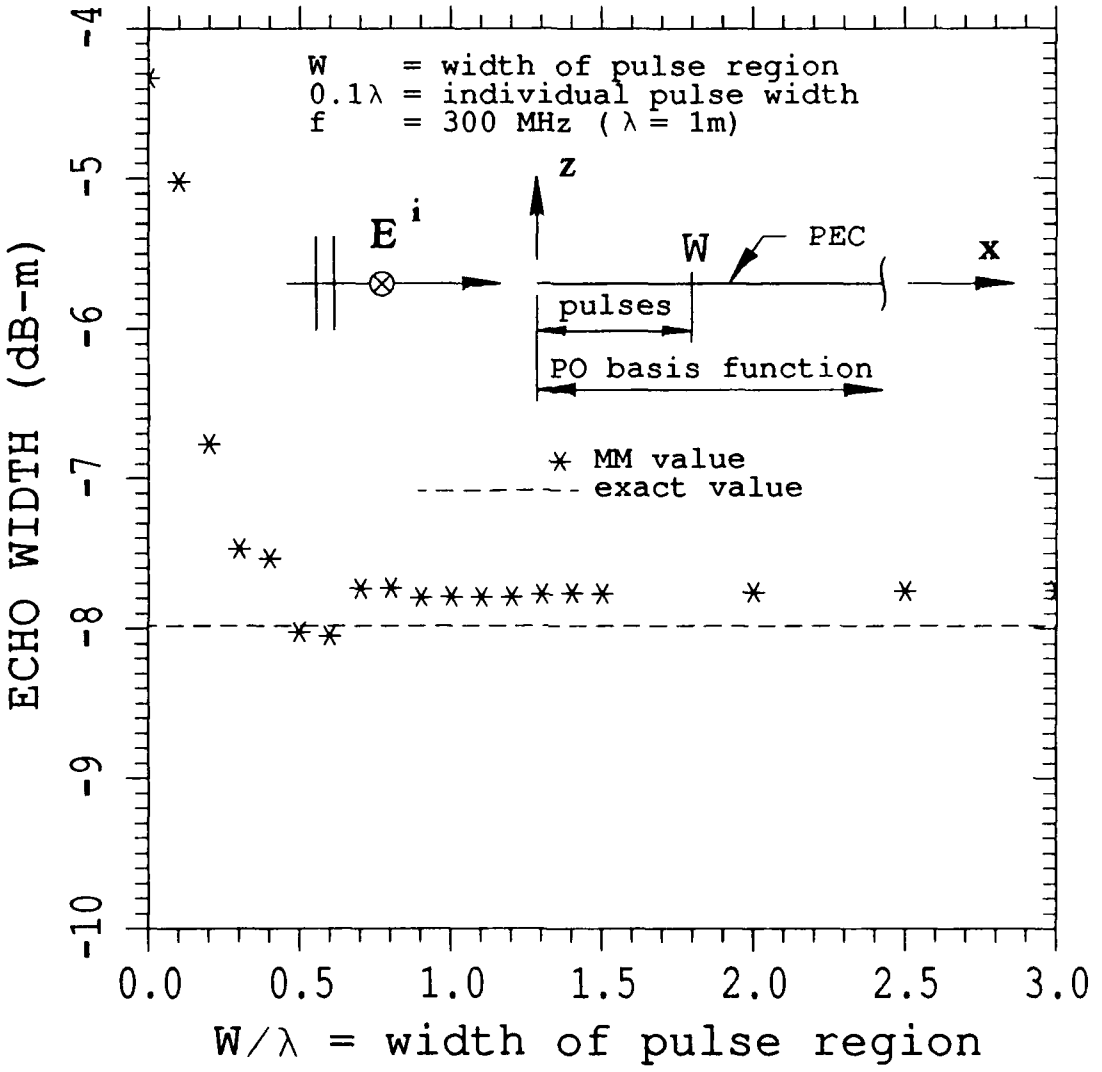

Figure 7: Convergence curve showing edge-on echo width versus pulse region width for PEC half plane.

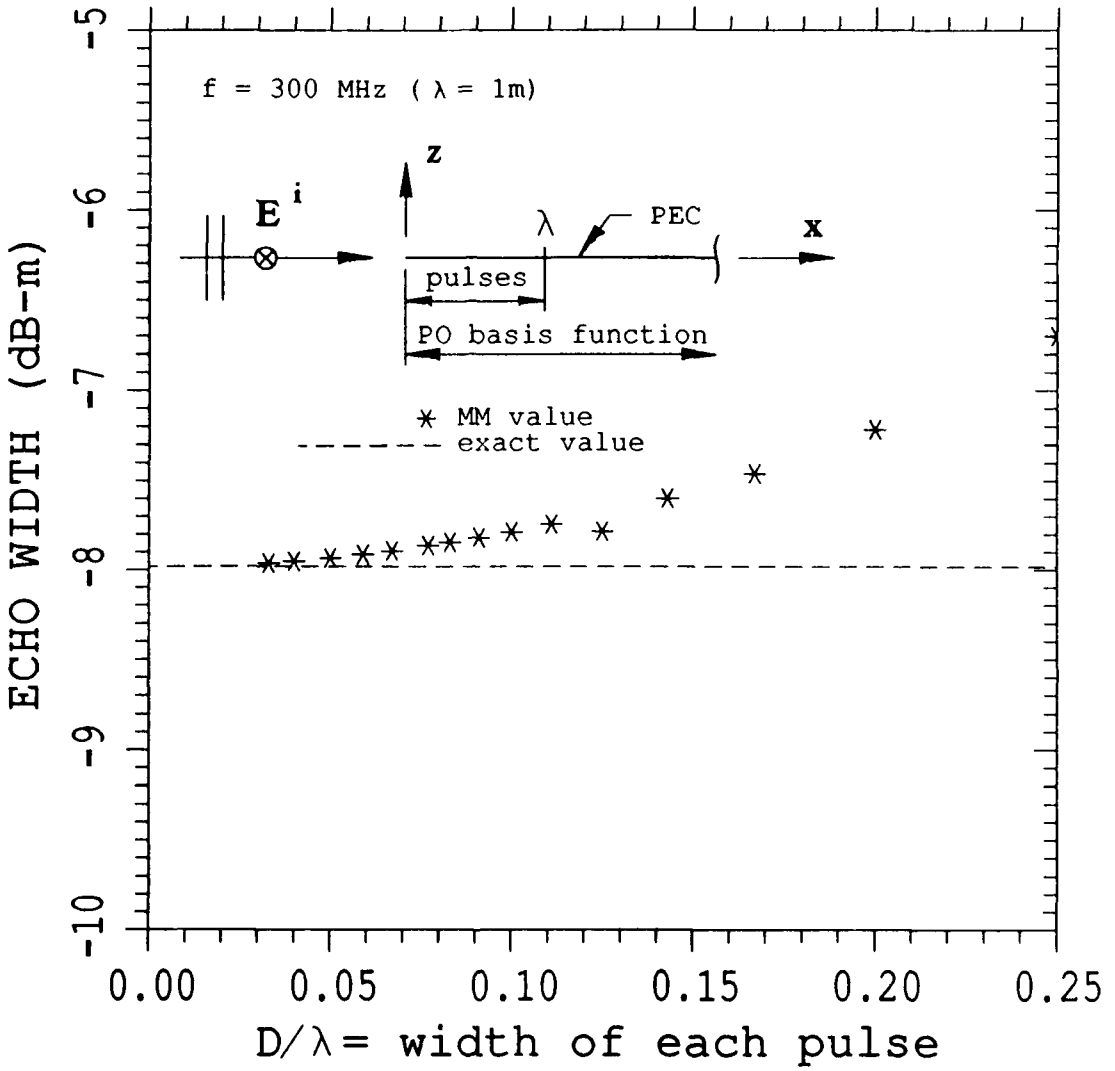

Figure 8: Convergence curve showing edge-on echo width versus individual pulse width for PEC half plane.

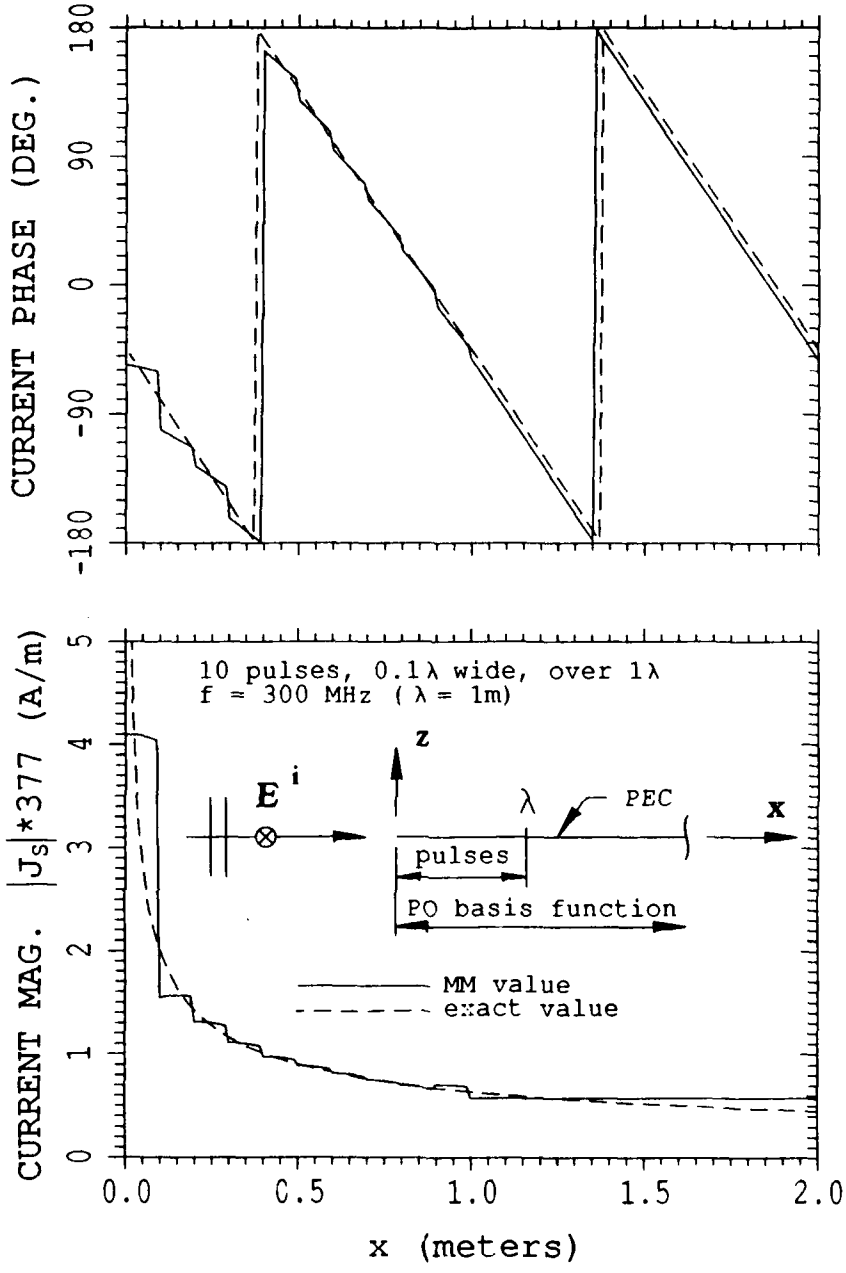

Figure 9: Comparison of MM current with exact current for edge-on incidence to a PEC half plane.

try analyzed here.

The geometry consists of a sheet impedance like that shown in Figure 3(b) given by Equation (2.2). Referring to Equation (2.2) the sheet impedance is defined by $Z_{S0} = 65\Omega$ and $Z_A = 0$ or ∞. The finite width where Z_A exists is $L = 7.62$cm. This sheet impedance is located in a $K = 2$ layered slab. Both layers are lossless and have permeability μ_0 and relative dielectric constant $\epsilon_r = 2.6$. The thickness of the layers is $T_1 = T_2 = 0.57$cm.

Figures 10 and 11 show plots of measured results compared with results obtained from this MM solution. Figure 10 corresponds to $Z_A = \infty$ and Figure 11 corresponds to $Z_A = 0$. The figures show backscatter versus frequency at $\phi_0 = 30°$. The MM computations were made using impedance matrix interpolation. The impedance matrix was computed every $\Delta f = 1$ GHz and echo width was calculated every $\Delta f = 25$ MHz. 33 pulse basis functions were used in the range from 4 to 8 GHz and 50 pulse basis functions were used from 8 to 12 GHz. This corresponds to a pulse width of about $0.1\lambda_D$ at the highest frequency in each range where λ_D is the wavelength in the dielectric layer. The solid curves are the calculated data and the dashed curves are the measured data. The results agree reasonably well, especially for $Z_A = \infty$. The data took about 22 minutes per plot to compute on a VAX 8550.

3.3 Backscatter From a Sheet Impedance in Free Space

This section presents backscatter from a sheet impedance half plane in free space. The geometry is sketched in the inserts of Figures 12 and 13. Several values for purely resistive and purely reactive sheet impedances are considered with backscatter patterns of their echo width included.

Figure 12 shows the computed backscatter echo width of a purely resistive

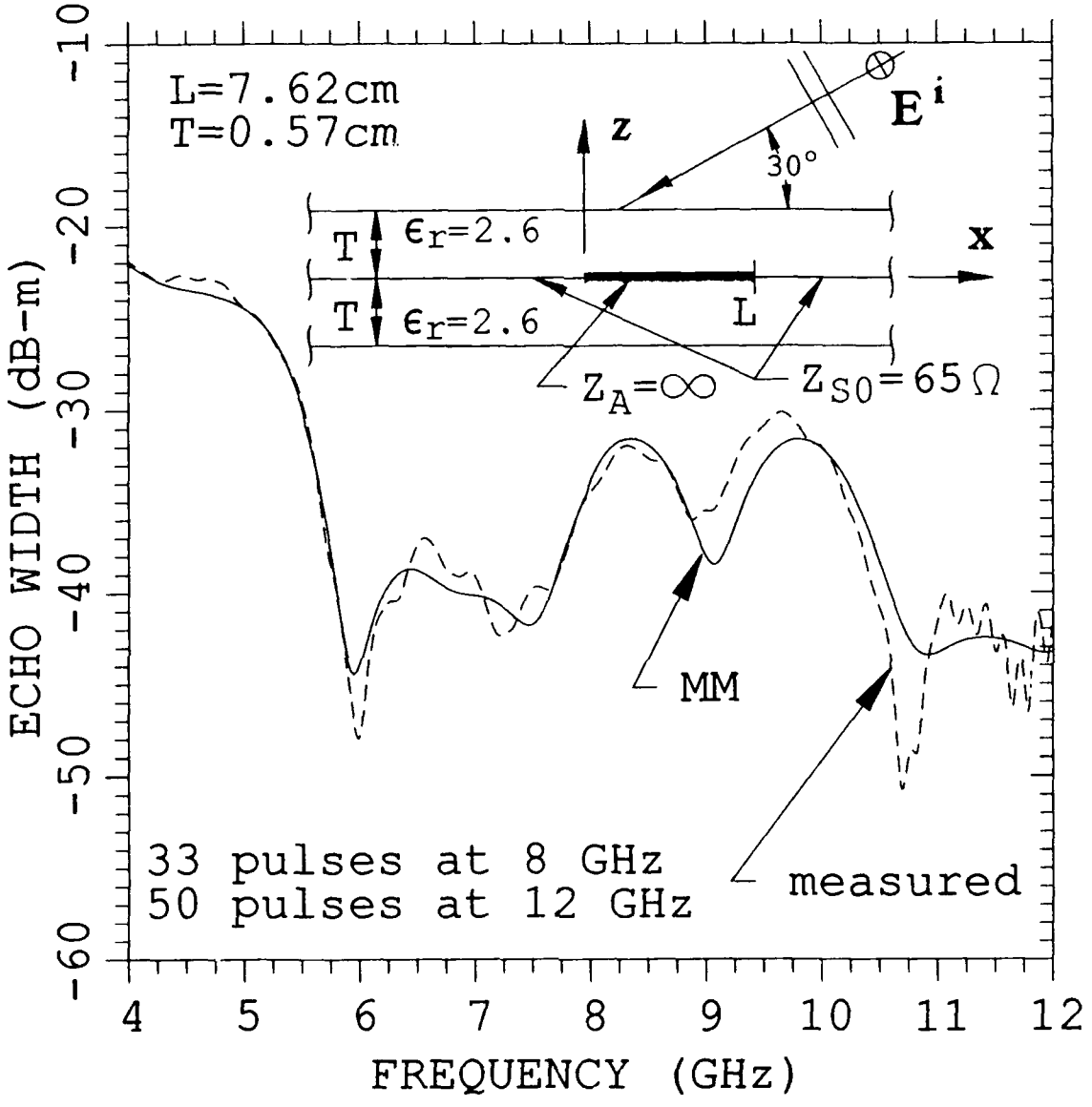

Figure 10: Backscatter by a sheet impedance located in a two layered slab. $Z_{S0} = 65\Omega$ and $Z_A = \infty$.

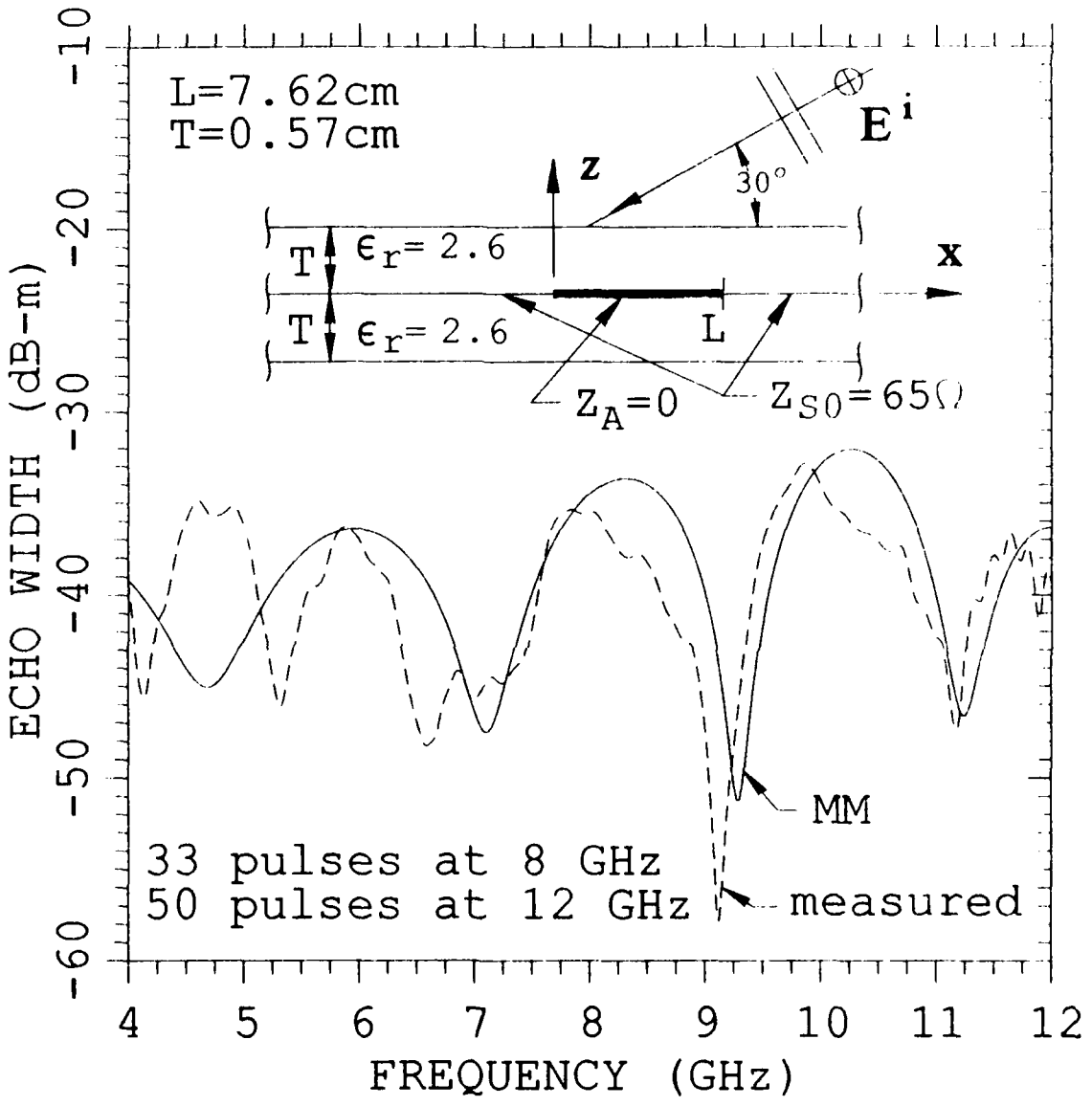

Figure 11: Backscatter by a sheet impedance located in a two layered slab. Z_{S0} = 65Ω and Z_A = 0.

sheet impedance half plane in free space. The sheet impedance is of the form shown in Figure 3(c) given in Equation (2.3) where $Z_{S0} = \infty$ and $Z_A = R_S$ with $R_S = 0, 100, 500, 2000, 10^4\Omega$. The echo width is given in dB-m and was calculated at 300.0 MHz. There were 10 pulse basis functions of width 0.1λ = 10cm each covering the first wavelength of the half plane. Furthermore, the PO basis function (starting at $x_{PO} = 0$) had to be included, making a total of 11 basis functions. No surface wave basis function was used since a purely real sheet impedance cannot support a surface wave. The edge-on backscatter at $\phi_0 = 180°$ is in excellent agreement with values previously calculated by Senior [5]. These points are indicated as large dots at 180° in Figure 12. Also, the MM results computed here check out very well against the asymptotic results of Ly [15]. Plots comparing these results were too similar to include here. The data in Figure 12 took about 28 minutes of CPU time to compute on a VAX 8550.

Similarly, Figure 13 shows the computed backscatter echo width of a purely reactive sheet impedance half plane in free space. The sheet impedance is of the same form given in Equation (2.3) where $Z_{S0} = \infty$ and $Z_A = -jX_S$ with $X_S = 0, 100, 500, 2000, 10^4\Omega$. The echo width is given in dB-m and was calculated at 300.0 MHz. There were 10 pulse basis functions of width 0.1λ = 10cm over the first wavelength of the half plane. The imaginary sheet impedance can support a surface wave so the surface wave basis function was included. It started at $x_S = 0$ and had propagation constant given by Equation (2.48). With the PO basis function, a total of 12 basis functions were used. The imaginary sheet impedance scattering results also check out very well with the work of Ly [15]. The data in Figure 13 took about 31 minutes to compute on a VAX 8550.

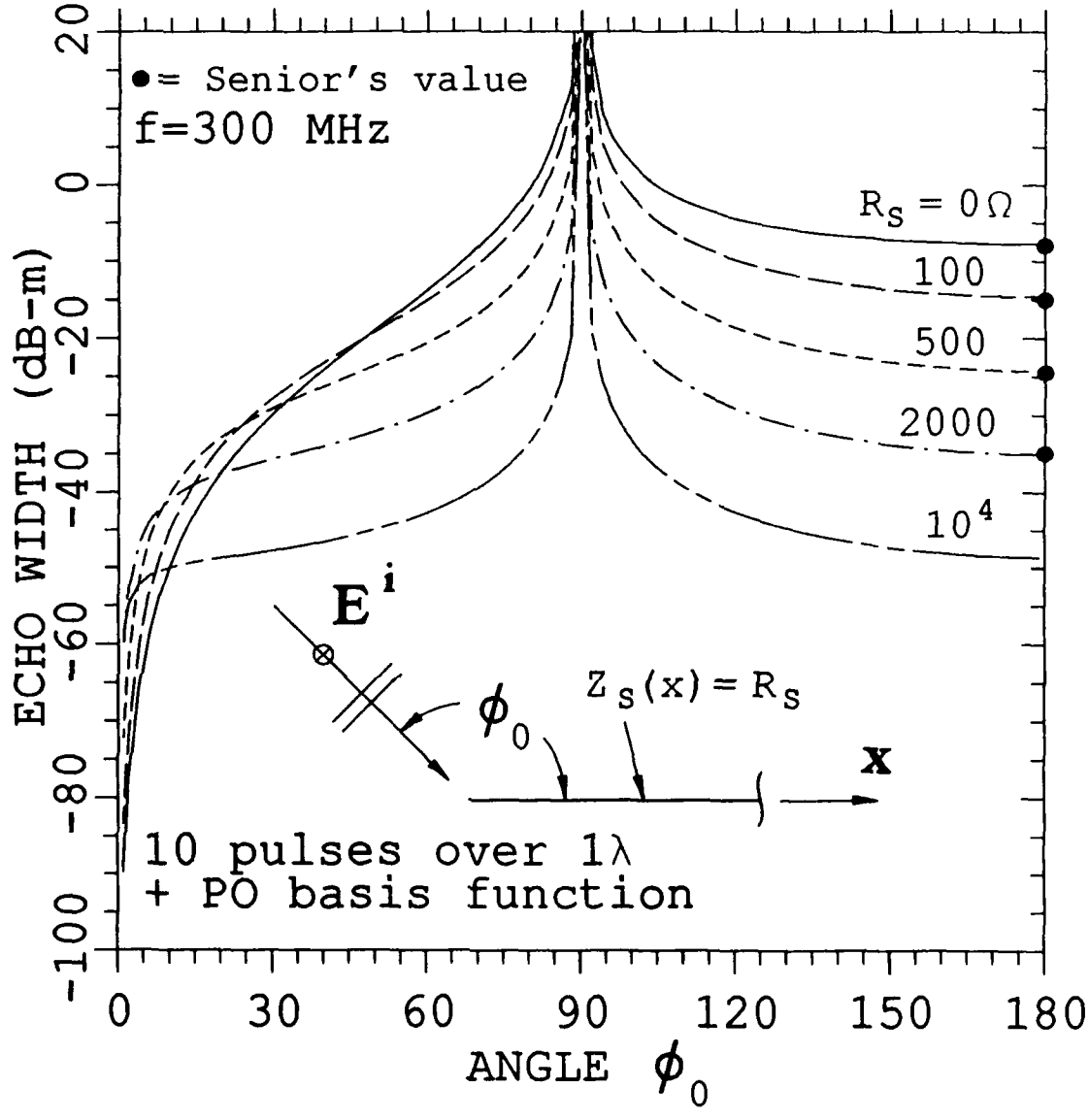

Figure 12: Backscatter by a purely real sheet impedance half plane in free space.

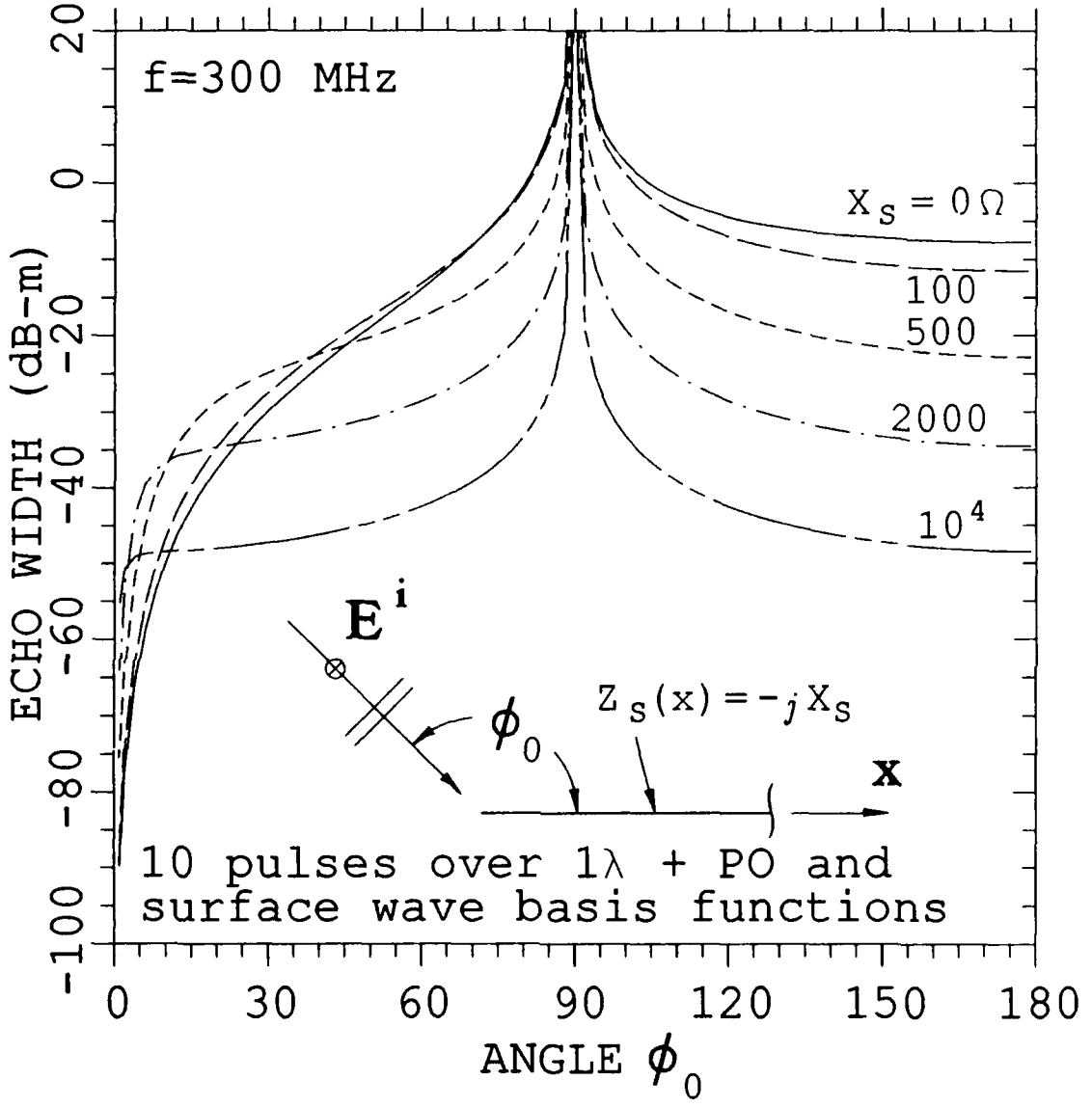

Figure 13: Backscatter by a purely imaginary sheet impedance half plane in free space.

3.4 Backscatter From a Tapered Sheet Impedance Half Plane in Free Space

This section presents results of backscatter from a tapered sheet impedance half plane in free space. The geometry is sketched in the insert of Figure 14 and the sheet impedance variation is described below. Backscatter patterns of echo width are included for several different linear impedance tapers. Also, backscatter patterns from a linearly tapered and a exponentially tapered sheet impedance are compared against results from Newman [8] [9].

The sheet impedance variation is similar to that shown in Figure 3(d) given by Equation (2.4). The sheet impedance tapers linearly from 1000Ω to 0Ω over the width L. For $x > L$ the sheet impedance is zero, i.e., a perfectly conducting half plane. Referring to Equation (2.4), the sheet impedance considered here is given as

$$Z_S(x) = \begin{cases} \infty & \text{if } x < 0 \\ 1000\left(1 - \frac{x}{L}\right) & \text{if } 0 \leq x \leq L \\ 0 & \text{if } x > L. \end{cases} \tag{3.1}$$

Backscatter patterns were computed for $L = 0, \lambda/4, \lambda/2, \lambda$ and 2λ. The backscatter patterns of echo width in dB-m are shown in Figure 14 and were computed at 300 MHz. In each case, pulse basis functions of width 0.05λ were placed over the impedance taper region and the first wavelength of the PEC, i.e., they were used from $x = 0$ to $x = L + \lambda$. The PO basis function had to be included and it started at $x_{PO} = 0$. The data of Figure 14 took about 145 minutes of CPU time on a VAX 8550.

For comparison, backscatter patterns from linearly tapered and exponentially tapered sheet impedances were compared with Newman's results. The width of the impedance taper region is $L = \lambda$ in both cases. The linear impedance taper

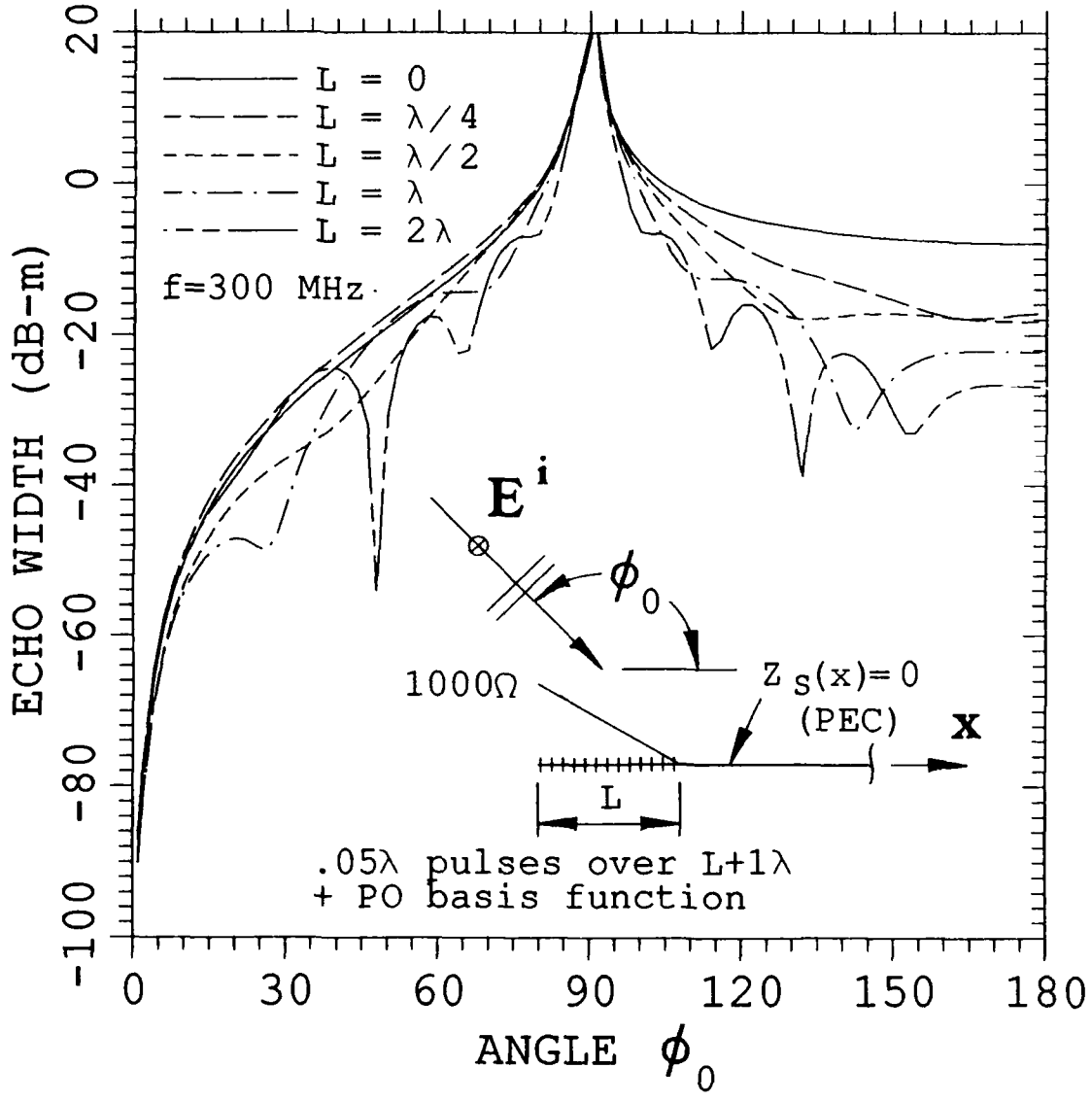

Figure 14: Backscatter by a linearly tapered sheet impedance half plane in free space.

is that of Equation (3.1). The exponential impedance tapers from 1000Ω to 10Ω exponentially and is given as

$$Z_S(x) = \begin{cases} \infty & \text{if } x < 0 \\ 10e^{-4.61(x-L)/\lambda} & \text{if } 0 \leq x \leq L \\ 0 & \text{if } x > L. \end{cases} \tag{3.2}$$

Figure 15 shows the results of this MM solution compared with Newman's results for both impedance tapers. The results are in good agreement, thus demonstrating the accuracy of this solution.

3.5 Backscatter From a Tapered Sheet Impedance Discontinuity in Free Space

This section presents results of backscatter from a tapered sheet impedance discontinuity in free space. The geometry is sketched in the insert of Figure 16. The problem considered in this section is similar to that of the previous section with the main difference being that the "background" impedance Z_{S0} is 100Ω instead of infinity. Backscatter patterns are included for several linear impedance tapers. Also, backscatter patterns from a linearly tapered and a cosinusoidally tapered sheet impedance are compared.

The sheet impedance tapers linearly from 100Ω to 0Ω over the width L and can be given by

$$Z_S(x) = \begin{cases} 100 & \text{if } x < 0 \\ 100\left(1 - \frac{x}{L}\right) & \text{if } 0 \leq x \leq L \\ 0 & \text{if } x > L. \end{cases} \tag{3.3}$$

Backscatter patterns were computed for $L = 0, \lambda/4, \lambda/2, \lambda$ and 2λ at 300 MHz and are shown in Figure 16. In each case, pulse basis functions of width 0.05λ were placed from $x = 0$ to $x = L + \lambda$. The PO basis function had to be included starting

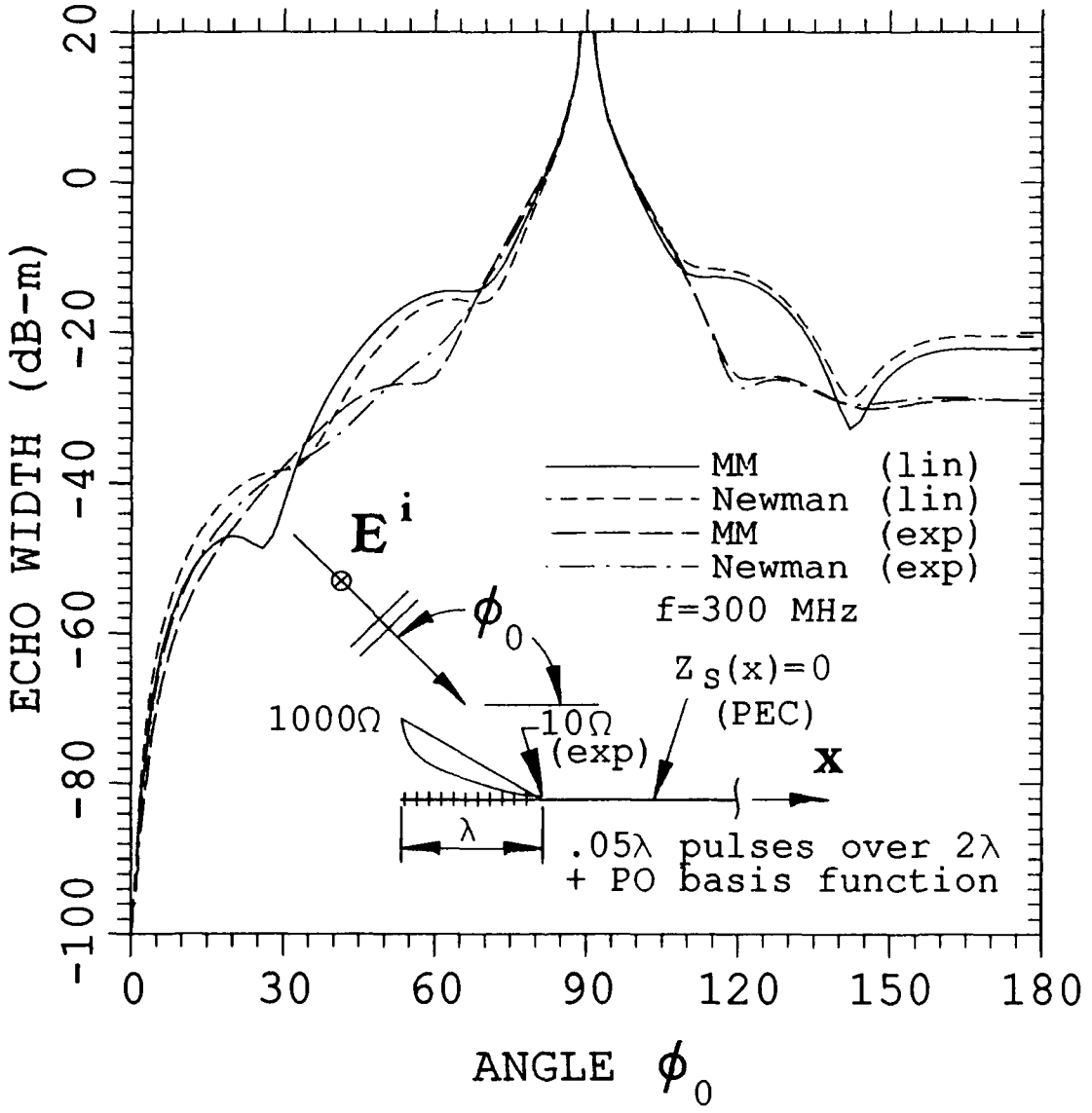

Figure 15: Comparison of backscatter by linearly and exponentially tapered sheet impedance half planes in free space.

at $x_{PO} = 0$. The data of Figure 14 took about 145 minutes of CPU time on a VAX 8550.

A cosinusoidal sheet impedance taper from 100Ω to 0Ω of width $L = \lambda$ was also analyzed. The cosinusoidal impedance taper is given as

$$Z_S(x) = 50 + 50\cos\left(\frac{\pi x}{L}\right) \quad \text{for } 0 \leq x \leq L. \tag{3.4}$$

The backscatter from this impedance taper is contrasted with the linear impedance taper of the same width in Figure 17. Both sheet impedances had the same basis function expansion of 40 pulse basis functions of width 0.05λ over the first 2 wavelengths. Both cases also used the PO basis function.

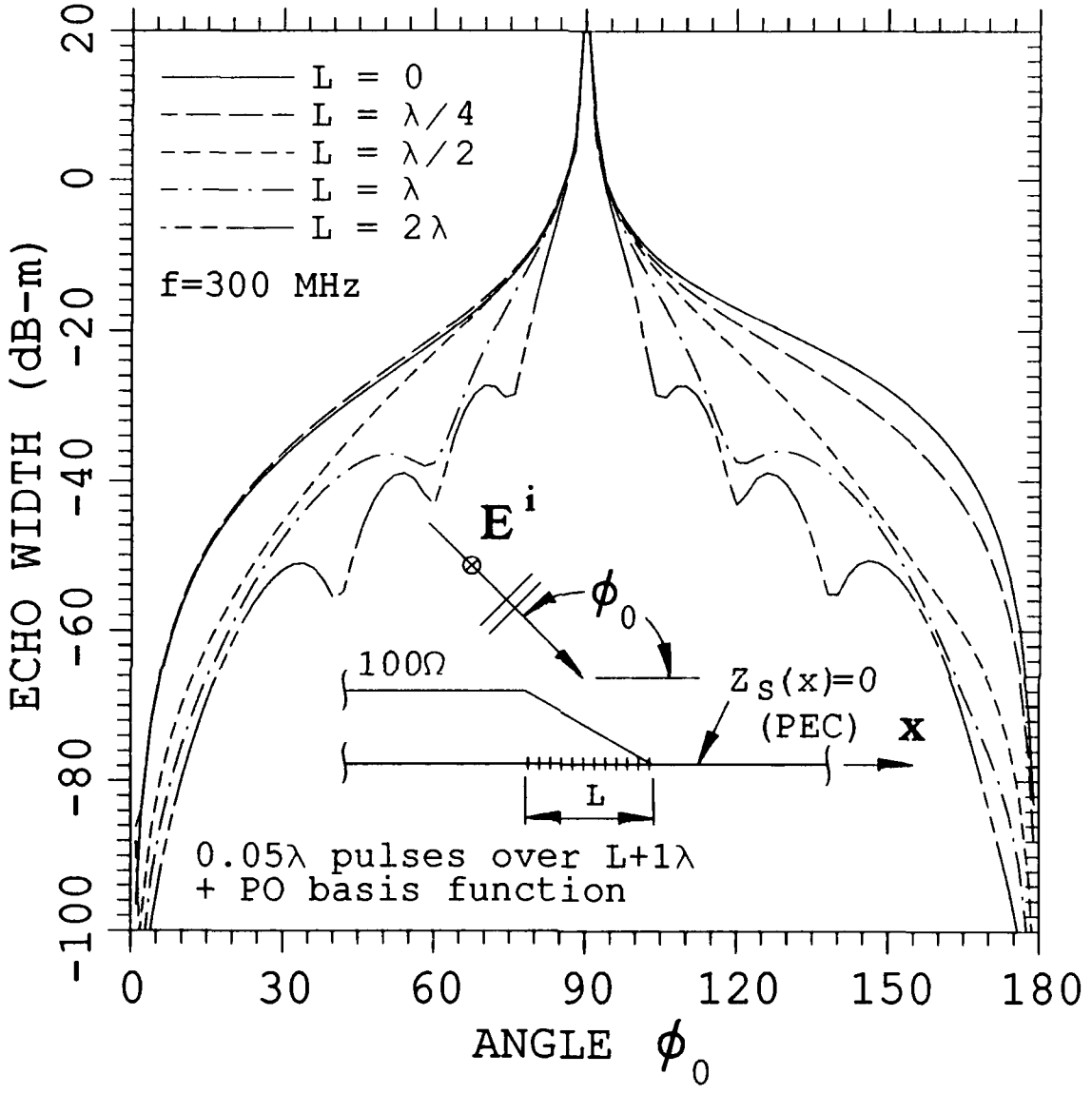

Figure 16: Backscatter by a linearly tapered sheet impedance discontinuity in free space.

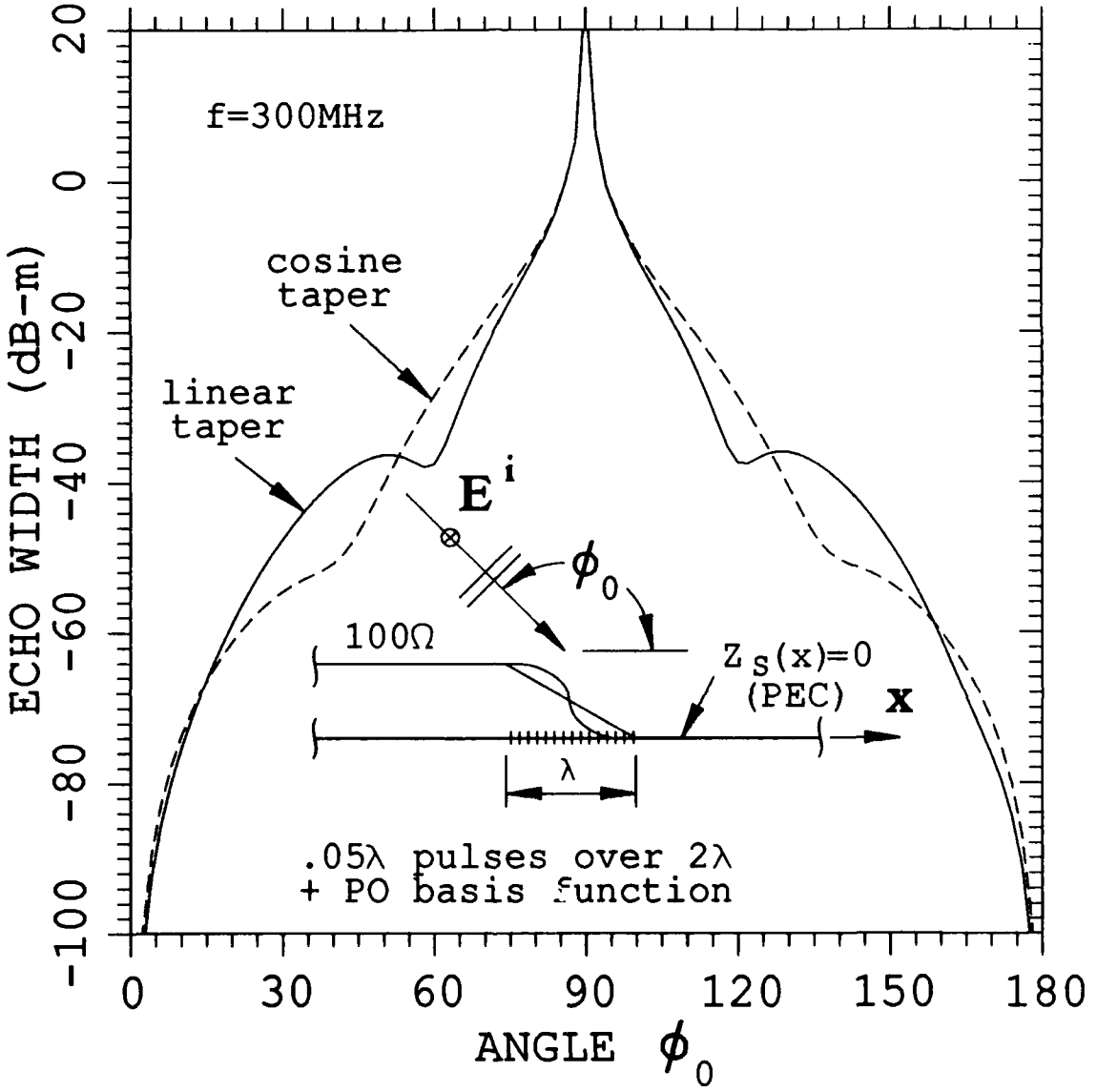

Figure 17: Comparison of backscatter by linearly and cosinusoidally tapered sheet impedance discontinuities in free space.

CHAPTER IV

DESCRIPTION OF COMPUTER CODE

This chapter describes briefly a computer code which implements the MM solution outlined in Chapter II. The computer code has been named the "$Z_S(x)$" Code (ZSX) by the author. ZSX can analyze the three multilayered slab geometries considered in Appendices A and B. These geometries are a sheet impedance located in a $K = 2$ layered slab, on a material half space, and in free space. ZSX can calculate bistatic or backscatter patterns, current distributions, and frequency sweep data. The inputs and outputs for ZSX are explained in this chapter.

4.1 Input and Output Files

ZSX utilizes one input file and two output files. The input file, INFIL.DAT, contains all the input data to ZSX, i.e., all the input data are read from INFIL.DAT. INFIL.DAT must be assigned to logical unit 8. The first output file, OUTFL.DAT, contains the output of ZSX. After a run, OUTFL.DAT contains the input data used in that run, the problem geometry and basis function expansion used, and a tabular listing of the electromagnetic calculations if any were made. OUTFL.DAT must be assigned to logical unit 9. The second output file, PTPLOT.DAT, contains tabular listings of the electromagnetic calculations. PTPLOT.DAT is intended for plotting purposes. PTPLOT.DAT will contain either a bistatic or backscatter pattern, a current distribution, or frequency sweep data.

```
C
C READ 1
      READ(8,*)NGO,IWRZM,IWRC,IGMTYP,IMF,IMS,IMP,NSH,BTMAX,ICALC
C
C READ 2
      READ(8,*)F
C
C READ 3A
      IF(IGMTYP.EQ.2)READ(8,*)ER1,TDE1,UR1,TDM1
C
C READS 3B AND 3C
      IF(IGMTYP.EQ.3)THEN
        READ(8,*)ER1,TDE1,UR1,TDM1,T1
        READ(8,*)ER2,TDE2,UR2,TDM2,T2
      ENDIF
C
C READ 4A
      READ(8,*)ZS0,ZS
C
C READ 4B
      READ(8,*)ITP,ZA,ZB,WD1
C
C READ 5
      READ(8,*)WD2,SGXW,X1,X2
C
C READ 6A
      IF(ICALC.EQ.0)READ(8,*)IPAT,DPHI,PHBST
C
C READ 6B
      IF((ICALC.EQ.1).OR.(ICALC.EQ.2))READ(8,*)FMC1,FMC2,DFZ,DFC,
     &PHIN,PHSC
C
C READ 6C
      IF(IPAT.EQ.3)READ(8,*)XI,XF,XS
```

Figure 18: The FORTRAN READ statements in ZSX.

PTPLOT.DAT must be assigned to logical unit 10.

4.2 Input Data

The input data to ZSX are explained in this section. The input data are used to describe to the program the problem geometry and indicate the desired electromagnetic calculations. The input data are obtained via FORTRAN READ statements. The READ statements and the parameters defined by them will be explained in this section. Figure 18 shows all the READ statements contained in ZSX. Note that not every READ statement will be executed in every program run. The input file, INFIL.DAT, contains the data to be read by the READ statements.

4.2.1 READ 1: Run Control Parameters

READ 1 defines the following run control parameters:

NGO = run indicator.

= 0 implies input and print out problem description and then stop, i.e., do not make any electromagnetic calculations.

= 1 implies input problem description and then perform the desired electromagnetic calculations. An NGO = 0 run should precede an NGO = 1 run as this allows the user to verify the accuracy of the problem description defined in the input file, INFIL.DAT.

IWRZM = indicator for writing the impedance matrix to the output file.

= 0 implies do not write the impedance matrix to the output file.

= 1 implies write the impedance matrix to the output file. Note that this will result in N^2 lines of output. Furthermore, the impedance matrix will be printed at every angle if a physical optics (PO) basis function is used and a backscatter pattern is defined.

IWRC = indicator for writing out both the voltage and current vector.

= 0 implies do not write out the voltage or current vector.

= 1 implies write out both the voltage and current vector. Note that for backscatter patterns this will result in the voltage and current vector being printed at every angle.

IGMTYP = indicator for the type of multilayered slab geometry.

= 1 implies a sheet impedance in free space.

= 2 implies a sheet impedance on a material half space.

= 3 implies a sheet impedance located in a $K = 2$ layered slab.

IMF = indicator for using a physical optics (PO) basis function.

= 0 implies do not use a PO basis fu ' on. Use this in the case that $Z_S(x) \neq Z_{S0}$ over a finite range of x.

= 1 implies use a PO basis function. Use this in the case that $Z_S(x) \neq Z_{S0}$ over a semi-infinite range of x.

IMS = indicator for using a surface wave basis function.

= 0 implies do not use a surface wave basis function.

= 1 implies use a surface wave basis function. IMS should be set equal to 1 only if: 1) the sheet impedance is NOT purely real and is in free space (IGMTYP = 1), and 2) the range where $Z_S(x) \neq Z_{S0}$ is semi- infinite. ZSX allows for only one surface wave basis function for the case that the sheet impedance is in free space. ZSX computes the surface wave propagation constant according to Equation (2.48).

IMP = indicator for using pulse basis functions.

= 0 implies do not use any pulse basis functions.

= 1 implies use pulse basis functions. This will almost always be the case.

NSH = number of Simpson's rule integration segments used per half cycle of the oscillatory part of the integrand of the spectral integral expression for Z_{mn} (Equation (2.31).) NSH = 4 typically but can be increased for greater accuracy.

BTMAX = upper and lower limits of integration used in the expression for Z_{mn} in terms of the maximum wavenumber of the multilayered slab materials, i.e., limits of integration for Equation (2.31) are $\pm$BTMAX$\times k_{D_{max}}$ where $k_{D_{max}}$ is the maximum wavenumber of any material in the multilayered slab.

BTMAX must be great enough to allow for convergence of the integral. BTMAX = 50.0 typically. To check for convergence, BTMAX can be increased until the impedance matrix elements are stable.

ICALC = indicator for performing frequency sweep computations.

= 0 implies do not perform a frequency sweep computation.

= 1 implies perform a frequency sweep computation using standard quadratic interpolation.

= 2 implies perform a frequency sweep computation using improved quadratic interpolation. This should never be done if a PO basis function is used (IMF = 1) or if a surface wave basis function is used (IMS = 1).

4.2.2 READ 2: Frequency

READ 2 defines F = the frequency in MHz at which any pattern or current distribution calculations are made. If a frequency sweep computation is desired, then the frequencies are determined via READ 6B. However, READ 2 will be executed in either case.

4.2.3 READ 3: Material Parameters

Note that READ 3A will be executed only if IGMTYP = 2 and that READ 3B and 3C will be executed only if IGMTYP = 3 (see READ 1). READ 3A determines the material parameters of the half space if IGMTYP = 2.

ER1 = relative real part of permittivity in material half space.

TDE1 = loss tangent of permittivity in material half space.

UR1 = relative real part of permeability in material half space.

TDM1 = loss tangent of permeability in material half space.

READ 3B and 3C determine the material parameters of the two-layered slab if IGMTYP = 3.

ER1 = relative real part of permittivity in layer $k = 1$.

TDE1 = loss tangent of permittivity in layer $k = 1$.

UR1 = relative real part of permeability in layer $k = 1$.

TDM1 = loss tangent of permeability in layer $k = 1$.

T1 = thickness in meters of layer $k = 1$.

ER2 = relative real part of permittivity in layer $k = 2$.

TDE2 = loss tangent of permittivity in layer $k = 2$.

UR2 = relative real part of permeability in layer $k = 2$.

TDM2 = loss tangent of permeability in layer $k = 2$.

T2 = thickness in meters of layer $k = 2$.

4.2.4 READ 4: Sheet Impedance

READ 4A defines the constant values of the sheet impedance $Z_S(x)$ as follows:

ZS0 = "background" constant sheet impedance Z_{S0}. If the user is interested in a case where $Z_{S0} \to \infty$, such as scattering from a resistive half plane in free space, then simply set ZS0 equal to a very large number. Experience has shown that ZS0 = 10^{25} gives good results in these cases.

ZS = constant value of the sheet impedance (not Z_{S0}) in the range where the sheet impedance is constant, but not equal to Z_{S0}. For example, set ZS = ZA for the sheet impedances shown in Figures 3(b), 3(c) and 3(d).

The width where $Z_S(x)$ is constant (not Z_{S0}) is taken to be finite if only pulse basis functions are used (see Figure 6(a).) This width is taken to be semi-infinite going to infinity in the $+\hat{x}$ - direction if a PO or surface wave basis function is used (see Figures 6(b) and 6(c).)

READ 4B can be used to define an impedance taper region. An impedance taper can account for a non-constant sheet impedance like that shown in Figure 3(d). ZSX can allow for only one sheet impedance taper. READ 4B defines the following:

ITP = indicator for an impedance taper.

= 0 implies do not include an impedance taper.

= 1 implies include a constant impedance taper.

= 2 implies include a linear impedance taper.

= 3 implies include an exponential impedance taper.

= 4 implies include a cosine impedance taper.

ZA = impedance value at the start of the impedance taper. ZA will be the value of a constant impedance taper if ITP = 1. Note that ZA input via this READ statement is not to be confused with Z_A of Figures 3 and 6.

ZB = impedance value at the end of the impedance taper.

WD1 = width in meters of the impedance taper region.

If ITP > 0 then there will be an impedance taper region. This impedance taper region starts at $x = -$WD1 and extends to $x = 0$. If ITP = 1 then the sheet impedance will have a constant value of ZA over this entire range of x. If ITP = 2,3 or 4 then the sheet impedance will have value ZA at $x = -$WD1 and value

ZB at $x = 0$. In these cases, the sheet impedance will taper from ZA to ZB either linearly, exponentially or cosinusoidally, depending on ITP.

4.2.5 READ 5: Basis Function Description

READ 5 defines the layout of the basis function expansion through the use of the parameters explained below.

WD2 = width of constant ZS where pulse basis functions will be used. This parameter has meaning only if IMP = 1. If IMP = 1 then pulse basis functions are placed from $x = 0$ to $x =$ WD2.

SGXW = maximum segment size of pulse basis functions in minimum wavelengths of a layer. SGXW should not exceed 0.25 but has typically been chosen as 0.1 or less.

X1 = the x value in meters where the physical optics basis function starts. X1 has meaning only if IMF = 1. X1 is analogous to x_{PO} of Equation (2.43) and is typically chosen as 0.0 or WD2.

X2 = the x value in meters where the surface wave basis function starts. X2 has meaning only if IMS = 1. X2 is analogous to x_S of Equation (2.46) and is typically chosen as 0.0 or WD2.

Note that if an impedance taper region is specified (ITP > 0 in READ 4B) then pulse basis functions are automatically placed over this region, i.e., if ITP > 0 then pulse basis functions are placed from $x = -$WD1 to $x = 0$. For pulse basis functions to be placed over the impedance taper region, IMP need not be set be set to 1 in READ 1. The width of these pulse basis functions over WD1 is determined by SGXW.

4.2.6 READ 6: Electromagnetic Calculations

Note that READ 6A is executed only if ICALC = 0 and READ 6B is executed only if ICALC = 1 or 2 (see READ 1). Similarly, READ 6C is executed only if IPAT = 3 in READ 6A. READ 6A specifies whether a pattern or a current distribution is to be computed. It also defines the pattern using the parameters explained below.

IPAT = indicator for computing either a pattern or a current distribution.

= 0 implies do NOT compute a pattern or a current distribution.

= 1 implies compute a backscatter pattern.

= 2 implies compute a bistatic scattering pattern.

= 3 implies compute a current distribution (see READ 6C).

DPHI = the angle increment for pattern computations. If IPAT = 1 or 2 the scattering pattern will be computed every DPHI degrees.

PHBST = the angle of the incident plane wave for bistatic scattering patterns or current distributions.

READ 6B defines a frequency sweep computation using the parameters explained below.

FMC1 = beginning frequency in MHz for a frequency sweep computation.

FMC2 = ending frequency in MHz for a frequency sweep computation.

DFZ = frequency step size in MHz for calculating the impedance matrix.

DFC = frequency step size in MHz for calculating the scattered field.

PHIN = angle of the incident field in degrees.

PHSC = angle of the scattered field in degrees.

If standard interpolation is used (ICALC = 1 in READ 1) then the frequency step size DFZ in MHz is typically set to $\Delta f_M/2$ where

$$\Delta f_M = \frac{300}{2L}\text{MHz}.$$

Here L is the width over which pulse basis functions are placed. Assuming that pulse basis functions are used (IMP = 1 in READ 1), then L = WD2 if no impedance taper is used (ITP = 0 in READ 4B) and L = WD1 + WD2 if an impedance taper is used (ITP > 0 in READ 4B). If improved interpolation is used (ICALC = 2 in READ 1) then DFZ can be increased to Δf_M or more. Recall that improved interpolation should not be used if either a PO or surface wave basis function is used.

READ 6C defines the current distribution via the parameters explained below.

XI = the initial value of x in meters for the current distribution.

XF = the final value of x in meters for the current distribution.

XS = the step size of x in meters for the current distribution.

If a current distribution is specified (IPAT = 3 in READ 6A) then the current induced by a plane wave incident from ϕ_0 = PHBST is computed. The current distribution is computed from x = XI to x = XF at increments of XS.

CHAPTER V

SUMMARY

This report has described the integral equation and MM solution for two-dimensional TM scattering by a variable sheet impedance in a multilayered slab. An integral equation was derived for the unknown surface current on the scattering portion of the sheet impedance. The moment method was applied to the integral equation to obtain an approximate expansion for the unknown surface current. Simple expressions for the impedance matrix and voltage vector elements used in the MM solution were obtained. The far field of the basis functions were determined asymptotically so the far zone scattered field could be obtained analytically. Numerical results were presented and some results were compared against measured or previously calculated results.

One important feature of this MM solution is that the impedance matrix elements and the far zone fields depend upon spectral functions specific to the geometry of the multilayered slab. Thus, different spectral functions can be used to apply the MM solution to different multilayered slab geometries. Spectral functions were obtained for a sheet impedance located in a $K - 2$ layered slab, on a material half space, or in free space. A user-oriented computer code was written to implement this MM solution and can account for the three geometries just mentioned. A user's manual for this code was given in Chapter IV.

Future work in this area might include the computation of transverse electric

(TE) scattering by the same geometries analyzed here. This solution will result in different spectral functions and will require different basis function expansions. Furthermore, the volume equivalence theorem applied to the thin dielectric slab may not be valid for near edge-on incidence, and this problem may have to be treated separately.

Another idea for further study is a more complete analysis of the surface wave poles and the surface wave basis functions. The MM solution presented in this report only used surface wave basis functions when the sheet impedance was in free space. If the dominant surface wave poles can be determined for more complicated layered geometries, then their corresponding surface wave basis functions can be included in the MM current expansions for these geometries.

APPENDIX A

THE DETERMINATION OF $F(\beta)$ FOR SEVERAL MULTILAYERED SLAB GEOMETRIES

This appendix derives the function $F(\beta)$ of Equation (2.29) for the two layered geometry shown in Figure 19. Equations (2.22) and (2.25) are used to express the electric field and the tangential magnetic field. The conditions on these fields, listed in Section 2.4, are enforced and the function $F(\beta)$ is solved for. From this result, the function $F(\beta)$ is also found for the two special limiting cases shown in Figure 20.

The electric field is expressed as

$$E_n^k(x,z) = \int_{-\infty}^{+\infty} \left[A_n^k(\beta)\, e^{-\gamma_k z} + B_n^k(\beta)\, e^{\gamma_k z} \right] e^{j\beta x}\, d\beta \qquad (A.1)$$

and the tangential magnetic field is expressed as

$$H_{nx}^k(x,z) = -\frac{1}{j\omega\mu_k} \int_{\infty}^{+\infty} \gamma_k \left[A_n^k(\beta)\, e^{-\gamma_k z} - B_n^k(\beta)\, e^{\gamma_k z} \right] e^{j\beta x}\, d\beta \qquad (A.2)$$

for k=0,1,2,3. γ_k is given by

$$\gamma_k = \sqrt{\beta^2 - k_k^2} \quad \text{where} \quad \begin{cases} k_k = \omega\sqrt{\mu_k \epsilon_k} \\ \mathrm{Re}(\gamma_k) \geq 0 \\ \mathrm{Im}(\gamma_k) \geq 0. \end{cases} \qquad (A.3)$$

The first condition on the fields is the radiation condition as $r \to \infty$. This implies that there are only upward travelling waves in region $k = 0$ and only

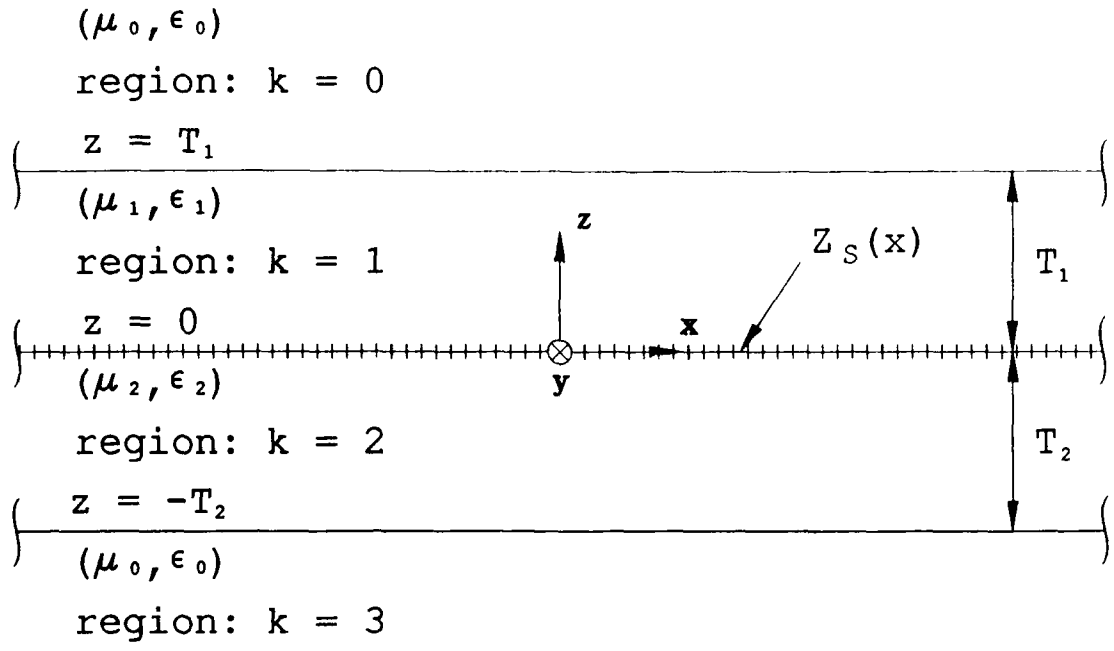

Figure 19: Sketch of two layered geometry containing sheet impedance $Z_S(x)$.

downward travelling waves in region $k = 3$. To enforce these properties, it must be true that

$$B_n^0(\beta) = 0 \quad \text{and} \quad A_n^3(\beta) = 0. \tag{A.4}$$

The second condition is continuity of the tangential electric field across each interface. Enforcing this condition yields the following:

$$\left[A_n^0(\beta)\, e^{-\gamma_0 T_1} \right] - \left[A_n^1(\beta)\, e^{-\gamma_1 T_1} + B_n^1(\beta)\, e^{\gamma_1 T_1} \right] = 0 \tag{A.5}$$

$$\left[A_n^1(\beta) + B_n^1(\beta) \right] - \left[A_n^2(\beta) + B_n^2(\beta) \right] = 0 \tag{A.6}$$

$$\left[A_n^2(\beta)\, e^{\gamma_2 T_2} + B_n^2(\beta)\, e^{-\gamma_2 T_2} \right] - \left[B_n^3(\beta)\, e^{-\gamma_3 T_2} \right] = 0. \tag{A.7}$$

The third condition is continuity of the tangential magnetic field across each interface except the $z = 0$ interface. Enforcing this condition yields the following:

$$-\frac{\gamma_0}{j\omega\mu_0} \left[A_n^0(\beta)\, e^{-\gamma_0 T_1} \right] + \frac{\gamma_1}{j\omega\mu_1} \left[A_n^1(\beta)\, e^{-\gamma_1 T_1} - B_n^1(\beta)\, e^{\gamma_1 T_1} \right] = 0 \tag{A.8}$$

$$-\frac{\gamma_2}{j\omega\mu_2}\left[A_n^2(\beta)\,e^{\gamma_2 T_2}-B_n^2(\beta)\,e^{-\gamma_2 T_2}\right]-\frac{\gamma_3}{j\omega\mu_3}\left[B_n^3(\beta)\,e^{-\gamma_3 T_2}\right]=0. \qquad (A.9)$$

The fourth and final condition is discontinuity of the tangential magnetic field, by the total surface current produced by J_n, across the $z = 0$ interface, i.e.,

$$\hat{\mathbf{z}}\times\left[\mathbf{H}_n^k-\mathbf{H}_n^{k+1}\right]=\mathbf{J}_n^t \qquad (A.10)$$

where k and $k+1$ represent the regions immediately above and below the $z = 0$ interface respectively, and $\mathbf{J}_n^t$ is the total surface current produced by J_n. Since $\mathbf{J}_n^t$ contains only a $\hat{y}$ - directed component, then for the $K = 2$ layered slab this condition becomes

$$H_{nx}^1-H_{nx}^2=J_n^t. \qquad (A.11)$$

The ($\hat{y}$ - polarized) surface current produced by J_n, at the $z = 0$ interface, is

$$J_n^t=\frac{E_n^1(x,0)}{Z_S(x)}=J_n+\frac{E_n^1(x,0)}{Z_{S0}}. \qquad (A.12)$$

Substituting Equations (2.20) and (A.1) into Equation (A.12) yields

$$J_n^t=\frac{1}{2\pi}\int_{-\infty}^{+\infty}\tilde{J}_n^-\,e^{j\beta x}\,d\beta+\frac{1}{Z_{S0}}\int_{-\infty}^{+\infty}\left[A_n^1(\beta)+B_n^1(\beta)\right]\,e^{j\beta x}\,d\beta. \qquad (A.13)$$

Enforcing the fourth condition by substituting Equations (A.2) and (A.13) into (A.11) yields

$$-\frac{\gamma_1}{j\omega\mu_1}\left[A_n^1(\beta)-B_n^1(\beta)\right]+\frac{\gamma_2}{j\omega\mu_2}\left[A_n^2(\beta)-B_n^2(\beta)\right]= \frac{1}{2\pi}\tilde{J}_n^-+\frac{1}{Z_{S0}}\left[A_n^1(\beta)+B_n^1(\beta)\right]. \qquad (A.14)$$

Equations (A.5) - (A.9) and (A.14) form a set of six equations that can be solved for the six unknown functions, $A_n^0(\beta)$, $A_n^1(\beta)$, $B_n^1(\beta)$, $A_n^2(\beta)$, $B_n^2(\beta)$, and $B_n^3(\beta)$. Of primary interest is the expression for the electric field at the $z = 0$ interface

$$E_n^1(x,0)=\int_{-\infty}^{+\infty}\left[A_n^1(\beta)+B_n^1(\beta)\right]\,e^{j\beta x}\,d\beta. \qquad (A.15)$$

Noting that regions $k = 0$ and $k = 3$ are the same media and solving Equations (A.5) - (A.9) and (A.14) for $A_n^1(\beta)$ and $B_n^1(\beta)$, Equation (A.15) becomes

$$E_n^1(x,0) = -\frac{1}{2\pi}\int_{-\infty}^{+\infty} F(\beta)\,\tilde{J}_n^-\,e^{j\beta x}\,d\beta \qquad (A.16)$$

where,

$$F(\beta) = \frac{\mu_1\gamma_0\,\sinh(\gamma_1 T_1) + \mu_0\gamma_1\,\cosh(\gamma_1 T_1)}{\left[C\mu_1\gamma_0 + \frac{\gamma_1}{j\omega\mu_1}\mu_0\gamma_1\right]\,\sinh(\gamma_1 T_1) + \left[C\mu_0\gamma_1 + \frac{\gamma_1}{j\omega\mu_1}\mu_1\gamma_0\right]\,\cosh(\gamma_1 T_1)} \qquad (A.17)$$

and

$$C = \frac{1}{Z_{S0}} + \frac{\gamma_2}{j\omega\mu_2}\left[\frac{\mu_2\gamma_0\,\cosh(\gamma_2 T_2) + \mu_0\gamma_2\,\sinh(\gamma_2 T_2)}{\mu_2\gamma_0\,\sinh(\gamma_2 T_2) + \mu_0\gamma_2\,\cosh(\gamma_2 T_2)}\right]. \qquad (A.18)$$

Now consider the geometry sketched in Figure 20(a). The geometry is a sheet impedance at $z = 0$ and bordered by free space (μ_0, ϵ_0) for $z > 0$ and material medium (μ_1, ϵ_1) for $z < 0$. This geometry can be considered a limiting case of the two layered geometry of Figure 19 where $T_1 \to 0$ and $T_2 \to \infty$. Since region $k = 2$ of Figure 19 becomes region $k = 1$ of Figure 20(a) then the $k = 2$ subscripts will become $k = 1$ subscripts. Performing these limiting operations on Equations (A.17) and (A.18) it is obtained that

$$F(\beta) = \frac{1}{\frac{1}{Z_{S0}} + \frac{\gamma_0}{j\omega\mu_0} + \frac{\gamma_1}{j\omega\mu_1}} \qquad (A.19)$$

for the geometry of Figure 20(a). If the sheet impedance is entirely in free space, as in Figure 20(b), then in Equation (A.19), $\mu_1 \to \mu_0$ and $\gamma_1 \to \gamma_0$. For this case, the function $F(\beta)$ is given by

$$F(\beta) = \frac{1}{\frac{1}{Z_{S0}} + \frac{2\gamma_0}{j\omega\mu_0}}. \qquad (A.20)$$

This ends the discussion on the calculation of $F(\beta)$.

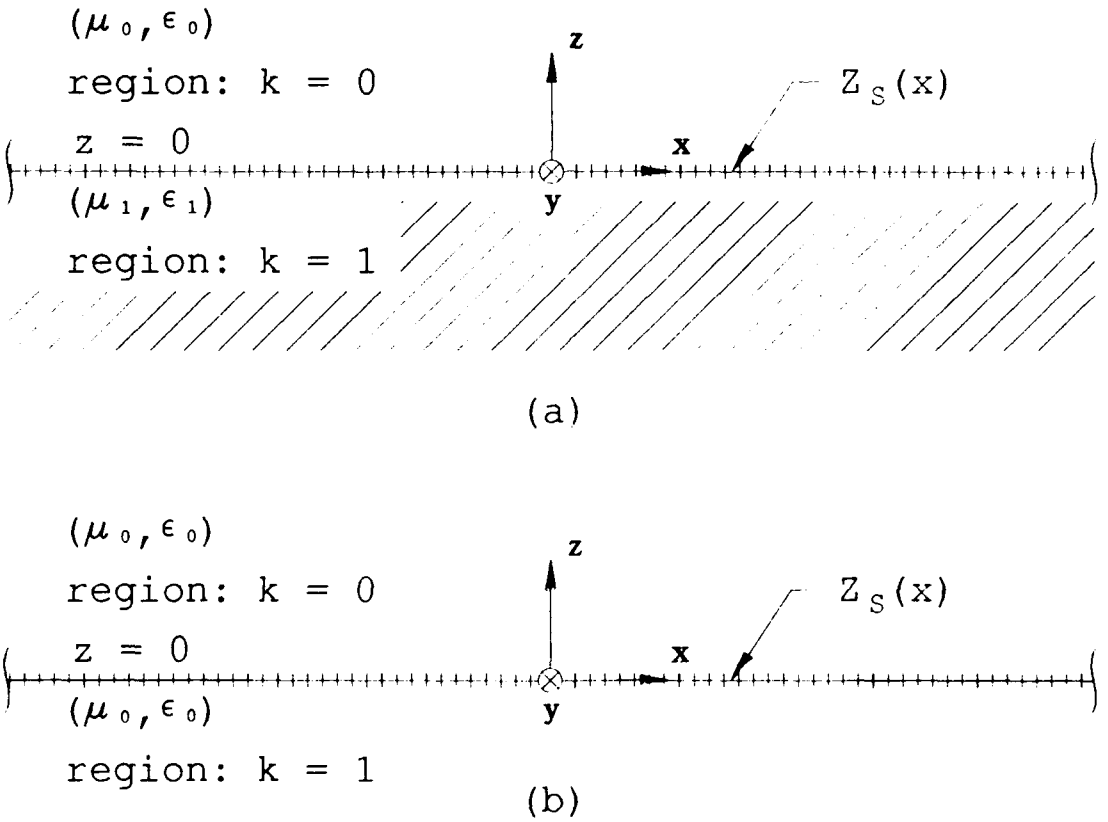

Figure 20: (a) Sketch of sheet impedance on a material half space. (b) Sketch of sheet impedance in free space.

APPENDIX B

THE DETERMINATION OF FAR ZONE FIELDS FOR SEVERAL MULTILAYERED SLAB GEOMETRIES

This appendix finds the far zone electric field of current expansion function J_m radiating in the presence of the multilayered slab. The electric field expression of Equation (2.22) for region $k = 0$ is evaluated asymptotically for $\rho \to \infty$ using the method of stationary phase. The result is given for the three geometries illustrated in Figures 19 and 20. The field is given only for region $k = 0$ above the multilayered slab, but by a similar approach, the field below the multilayered slab can be obtained.

The first order asymptotic approximation to the integral [18]

$$I(\lambda) = \int_a^b f(t)\, e^{j\lambda\,\psi(t)}\, dt \qquad (B.1)$$

for $\lambda \to \infty$ and $\psi'(c) = 0$ with $a < c < b$ and c not too close to a and b, is

$$I(\lambda) \approx f(c) \sqrt{\frac{2\pi}{\lambda|\psi''(c)|}}\, e^{j\lambda\psi(c)}\, e^{j\frac{\pi}{4}\,\mathrm{sgn}\,\psi''(c)}. \qquad (B.2)$$

Employing Equations (2.22) and (A.4), the field for region $k = 0$ above the multilayered slab is

$$E_m^0(x,z) = \int_{-\infty}^{+\infty} A_m^0(\beta)\, e^{-\gamma_0 z}\, e^{j\beta x}\, d\beta. \qquad (B.3)$$

To get this expression in the form of Equation (B.1) the following substitutions are made:

$$x = \rho\cos\phi$$

$$z = \rho \sin\phi$$

$$\gamma_0 = \sqrt{\beta^2 - k_0^2} = j\sqrt{k_0^2 - \beta^2}$$

yielding

$$E_m^0(\rho,\phi) = \int_{-\infty}^{+\infty} A_m^0(\beta)\, e^{j\rho\left[\beta\cos\phi - \sqrt{k_0^2-\beta^2}\,\sin\phi\right]}\, d\beta. \qquad (B.4)$$

Using Equation (B.2) with

$$t \rightarrow \beta$$

$$\lambda \rightarrow \rho$$

$$a \rightarrow -\infty$$

$$b \rightarrow +\infty$$

$$f(t) \rightarrow A_m^0(\beta)$$

$$\psi(t) \rightarrow \beta\cos\phi - \sqrt{k_0^2 - \beta^2}\,\sin\phi$$

$$c \rightarrow \beta_{sp} = -k_0\cos\phi$$

where β_{sp} is the stationary phase point, it is obtained that

$$E_m^0(\rho,\phi) = P_m(\phi)\,\frac{e^{-jk_0\rho}}{\sqrt{\rho}} \qquad (B.5)$$

where

$$P_m(\phi) = A_m^0(-k_0\cos\phi)\,\sqrt{2\pi k_0}\,\sin\phi\, e^{j\frac{\pi}{4}}. \qquad (B.6)$$

Note that the spectral function $A_m^0(\beta)$ is the only term in the expression for E_m^0 that depends on the multilayered slab geometry. This makes it straightforward to find the far zone field of a basis function radiating in the presence of a new multilayered slab geometry. The $A_m^0(\beta)$ corresponding to the new geometry must be determined and then inserted into Equation (B.6).

The function $A_m^0(\beta)$ can be found by enforcing the conditions on the fields given in Section 2.4 and following an approach similar to that outlined in Appendix A. The result of this operation is that for the two layered geometry of Figure 19

$$A_m^0(\beta) = \frac{\left[-\frac{1}{2\pi}\tilde{J}_m^-\right]\mu_0\gamma_1 e^{\gamma_0 T_1}}{\left[C\mu_1\gamma_0 + \frac{\gamma_1}{j\omega\mu_1}\mu_0\gamma_1\right]\sinh(\gamma_1 T_1) + \left[C\mu_0\gamma_1 + \frac{\gamma_1}{j\omega\mu_1}\mu_1\gamma_0\right]\cosh(\gamma_1 T_1)} \tag{B.7}$$

where

$$C = \frac{1}{Z_{S0}} + \frac{\gamma_2}{j\omega\mu_2}\left[\frac{\mu_2\gamma_0\cosh(\gamma_2 T_2) + \mu_0\gamma_2\sinh(\gamma_2 T_2)}{\mu_2\gamma_0\sinh(\gamma_2 T_2) + \mu_0\gamma_2\cosh(\gamma_2 T_2)}\right]. \tag{B.8}$$

The geometry of Figure 20(a) can be considered the limiting case of the two layered geometry of Figure 19 where $T_1 \to 0$ and $T_2 \to \infty$. Since region $k = 2$ of Figure 19 becomes region $k = 1$ of Figure 20(a) then the $k = 2$ subscripts will become $k = 1$ subscripts. Performing these limiting operations on Equations (B.7) and (B.8) it is obtained that

$$A_m^0(\beta) = \frac{-\frac{1}{2\pi}\tilde{J}_m^-}{\frac{1}{Z_{S0}} + \frac{\gamma_0}{j\omega\mu_0} + \frac{\gamma_1}{j\omega\mu_1}} \tag{B.9}$$

for the geometry of Figure 20(a). If the sheet impedance is entirely in free space, as in Figure 20(b), then in Equation (B.9), $\mu_1 \to \mu_0$ and $\gamma_1 \to \gamma_0$. For this case, the function $A_m^0(\beta)$ is given by

$$A_m^0(\beta) = \frac{-\frac{1}{2\pi}\tilde{J}_m^-}{\frac{1}{Z_{S0}} + \frac{2\gamma_0}{j\omega\mu_0}}. \tag{B.10}$$

To obtain a closed form expression for the far zone electric field above the multilayered slab, the function $A_m^0(\beta)$ is evaluated at $\beta = \beta_{sp} = -k_0\cos\phi$. $A_m^0(\beta_{sp})$ is substituted into Equation (B.6), which is then substituted into Equation (B.5) yielding a closed form expression for E_m, the far zone field of current expansion function J_m. E_m is then used in the evaluation of the voltage vector elements of Equation (2.36) and for finding the total far zone scattered field. This ends the discussion on evaluating E_m.

BIBLIOGRAPHY

[1] R.F. Harrington, Field Computations by Moment Methods, Robert E. Krieger Publishing Company, Malabar, Florida, 1968.

[2] R.F. Harrington, "Matrix Methods for Field Problems," Proceedings of the IEEE, Vol. 50, February 1967, pp. 136-149.

[3] E.H. Newman, "An Overview of the Hybrid MM/Green's Function in Electromagnetics," Proceedings of the IEEE, Vol. 76, March 1988, pp. 270-282.

[4] R.F. Harrington and J.R. Mautz, "An Impedance Sheet Approximation for Thin Dielectric Shells," IEEE Trans., Vol. AP-23, July 1975, pp. 531-534.

[5] T.B.A. Senior, "Half-Plane Edge Diffraction," Radio Science, Vol. 10, June 1975, pp. 645-650.

[6] T.B.A. Senior, "Backscattering from Resistive Strips," IEEE Trans., Vol. AP-27, November 1979, pp. 808-813.

[7] J.H. Richmond, "Scattering by Thin Dielectric Strips," IEEE Trans., Vol. AP-33, January 1985, pp. 64-68.

[8] E.H. Newman, "TM Scattering by a Dielectric Cylinder in the Presence of a Half Plane," IEEE Trans., Vol. AP-33, July 1985, pp. 773-782.

[9] E.H. Newman, "TM and TE Scattering by a Dielectric/Ferrite Cylinder in the Presence of a Half Plane," IEEE Trans., Vol. AP-34, June 1986, pp.804-813.

[10] E.H. Newman and J.L. Blanchard, "TM Scattering by an Impedance Sheet Extension of a Parabolic Cylinder," IEEE Trans., Vol. AP-36, April 1988, pp. 527-534.

[11] R.G. Kouyoumjian and P.H. Pathak, "A Uniform Geometrical Theory of Diffraction for an Edge in a Perfectly Conducting Surface," Proceedings of the IEEE, Vol. 62, November 1974, pp.1448-1461.

[12] R.G. Rojas, "A Uniform GTD Analysis of the EM Diffraction by a Thin Dielectric/Ferrite Half-Plane and Related Configurations," Ph.D. Dissertation, The Ohio State University Dept. of Elec. Engr., Columbus, Ohio, March 1985.

[13] R.G. Rojas and P.H. Pathak, "Diffraction of EM Waves by a Dielectric/Ferrite Half-Plane and Related Configurations," IEEE Trans., Vol. AP-37, June 1989, pp. 751-763.

[14] R.G. Rojas, "Weiner-Hopf Analysis of the EM Diffraction by an Impedance Discontinuity in a Planar Surface and a Half-Plane," IEEE Trans., Vol. AP-36, January 1988, pp. 71-83.

[15] H.C. Ly, "A UTD Analysis of the Diffraction by Planar Two and Three Part Configurations Consisting of Thin Dielectric/Ferrite Materials," M.S. Thesis, The Ohio State University Dept. of Elec. Engr., Columbus, Ohio, March 1989.

[16] R.F. Harrington, Time-Harmonic Electromagnetic Fields, McGraw-Hill, New York, 1961.

[17] B.W. Kwan, "Mutual Coupling Analysis for Conformal Microstrip Antennas," Ph.D. Dissertation, The Ohio State University Dept. of Elec. Engr., Columbus, Ohio, December 1984.

[18] N. Bleistein and R.A. Handelsman, Asymptotic Expansions of Integrals, Dover Publications, Inc., New York, 1975, pp. 219-224.

[19] J.H. Richmond, "Propagation of Surface Waves on a Thin Resistive Sheet or a Coated Substrate," Radio Science, Vol. 22, May 1987, pp. 825-831.

[20] E.H. Newman, "Generation of Wideband Data from the Method of Moments by Interpolating the Impedance Matrix," IEEE Trans., Vol. AP-36, December 1988, pp. 1820-1824.